UNIVERSITY OF NEW MEXICO
ALBUQUERQUE

# ENGINEERING EXPERIMENT STATION

Technical Report EE-59

## A MODELING TECHNIQUE FOR EXPERIMENTAL VERIFICATION OF DIPOLE RADIATION IN A CONDUCTING HALF SPACE

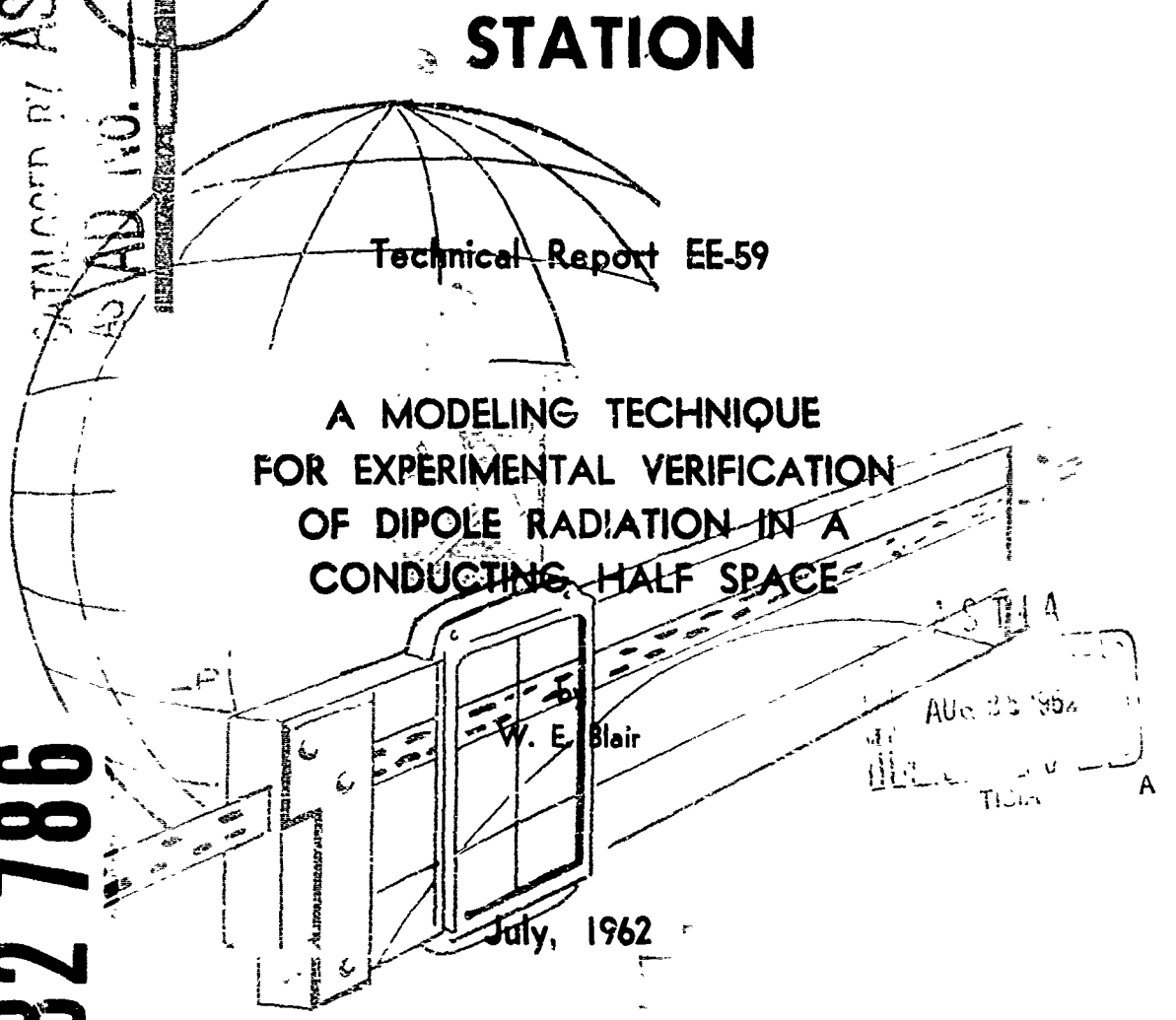

By
W. E. Blair



July, 1962



This work performed under
Contract Nonr 2798(01)

Engineering Experiment Station
University of New Mexico
Albuquerque, New Mexico

# A MODELING TECHNIQUE FOR EXPERIMENTAL VERIFICATION OF DIPOLE RADIATION IN A CONDUCTING HALF SPACE

by

W. E. Blair*

*E.E. Department
University of New Mexico
Albuquerque, New Mexico

This work was performed under
Contract Nonr 2798(01)

## ABSTRACT

A laboratory-size model of the flat earth-air (two-layer) problem, constructed to verify certain proposed theories on electromagnetic propagation through the sea, is described. The modeling system and technique is used in scaling and measuring electromagnetic field components of electric or magnetic antennas submerged in sea water.

Specifically, the experimental results are compared with the theory of radiation from a horizontal electric dipole antenna submerged in the sea, representing a conducting half-space. The results agree well with the theory within the valid range of variation of the parameters and in some cases even beyond this range. The results presented here verify (1) that the cylindrical coordinate $E_r$ and $E_\rho$ field components measured in the sea vary with radial distance from the antenna as $\rho^{-3}$ in the near zone and $\rho^{-1}$ and $\rho^{-2}$, respectively, in the far-zone; (2) all field components vary with depth, z, as $\exp(-z/\delta)$, where $\delta$ is skin depth; (3) the $E_r$ and $E_\phi$ components vary with $\phi$ as $\cos\phi$ and $\sin\phi$, respectively; (4) all field components vary linearly with length, $\ell$, and dipole current, I. In addition, the $H_\phi$, $H_r$, and $E_z$ components were measured in the air as a function of $\rho$ for the static-zone, near-zone, and far-zone.

The modeling system representing the sea includes a cylindrical tank 12' diameter, 2' deep, containing a salt solution of 4 mhos/meter conductivity. The transmitting

frequency varied from 100 to 400 mc/s. For antennas that can be validly scaled at least $10^{-2}$ in size and $10^{-4}$ in frequency, this model can conveniently be used to verify experimentally the radiation from these antennas when they are submerged in the sea.

TABLE OF CONTENTS

# A MODELING TECHNIQUE FOR EXPERIMENTAL VERIFICATION OF DIPOLE RADIATION IN A CONDUCTING HALF SPACE

## 1.0 Introduction

For many years, in addition to propagation through the atmosphere, scientists and engineers have been interested in the nature of propagation of electromagnetic energy through the earth (ground or sea). For purposes of communication, propagation through the troposphere was accepted as the most desirable because radio frequency energy is too rapidly attenuated when propagated through the sea, ground, and even under certain conditions through the ionosphere. However, following the acceptance of the submarines in naval warfare, expecially the atomic submarine, it has been vitally important to develop a theory and technique for communication between submerged submarines; that is, communication through the sea.

A number of theories on electromagnetic propagation through the sea and submerged antenna design have been proposed for communication purposes. Most of the valid theories have been verified either by using submarines directly or by some modeling procedure. The purpose of this report is (1) to describe a laboratory model for testing antenna impedance and propagation characteristics; (2) to verify the theory of the radiation of a submerged horizontal electric dipole.

The present theory of communication between two arbitrary points near the surface of the earth was originated by

Sommerfeld [1909; 1926] and Weyl [1919]. However, these and other early theoretical investigators considered the problem of the transmitting antenna as well as the receiving antenna on or above the surface of the earth.

Although many investigators worked with buried and submerged antennas before 1940, few reliable results were published. The first extensive theoretical and experimental work was conducted by the Naval Research Laboratory, Washington, D. C., [Norgorden, 1940; Isely, 1941]. Norgorden was probably first to analyze the insulated loop submerged in sea water; he determined theoretically and experimentally that horizontal antennas were superior in the sea (compared to vertical antennas being superior in the air). He also determined the variation of received signals as functions of frequency, field strengths in air above the loop, depth, and Q of the loop.

Isely experimentally investigated field strengths and noise levels of various types of submerged receiving antennas at different frequencies. He determined that signal strength increased with lower frequencies. Fratianni [1946; 1948] investigated various methods of coupling submerged loops to submarine receivers. The possibility of using a submerged loop for transmitting signals was also considered by Quinn and Norgorden [1946].

In addition to the work on magnetic antennas theoretical and experimental work on the horizontal electric antenna was initiated by investigators at the Naval Research Laboratory [Flath, 1949]. Flath and Norgorden determined the input impedance of an electric coaxial transmission line; then Appleman

[1951] experimentally verified Flath's and Norgorden's results. In a dissertation Moore [1951] analyzed communication using two submerged antennas and considered all four antenna configurations (vertical and horizontal; electric and magnetic). He also derived the impedances for these antenna configurations, and his results agree with those of Flath and Norgorden.

Extensive modeling of horizontal electric antennas verifying Norgorden's and Moore's theory has been conducted by Musselman [1953], Musselman and Roos [1955], Rauen [1953], and Snodgrass and Rudnick [1954]. Musselman tested the horizontal electric antenna as a receiving and transmitting antenna, investigating impedances, efficiencies and other parameters. Rauen tested the horizontal electric antenna as a submerged transmitting antenna.

A rigorous mathematical analysis of the horizontal electric dipole in a semi-infinite conducting medium is presented by Baños and Wesley [1953; 1954]. Some of the results of Moore and Baños and Wesley have been verified experimentally. Near-zone magnetic field intensity from submerged dipoles was measured by Kraichman [1960]; and the exponential variation of electric field strength with depth was measured by Saran and Held [1960]. Wait has written several papers on dipole radiation in a semi-infinite, conducting medium, including a recent summary paper of accepted theories [Wait, 1961]. Moore's analysis has been summarized and is available in a recent paper by Moore and Blair [1961].

## 2.0 Theoretical Relations for Submerged Dipole Radiation

The above-mentioned theoretical and experimental results indicate that the submerged horizontal electric dipole is best for transmitting and receiving electromagnetic energy in the sea. That is, qualitatively, the electromagnetic energy density, at some arbitrary point of observation (in near-zone or far-zone) in the sea, is largest if the transmitting dipole is a horizontal dipole.

The mode of communication can be described qualitatively as follows:

i. electromagnetic fields, radiated in the sea by a submerged transmitting dipole, are attenuated rapidly (exponentially); the fraction of the energy that reaches the surface directly above the transmitting antenna refracts into the air and establishes effectively a vertically polarized electric wave;

ii. this wave appears as if it originated from a vertical electric dipole located on the surface directly over the actual submerged transmitting dipole, and travels outward along the surface attenuating radially; moreover, this wave is weighted by cos $\phi$, where $\phi$ is measured from the horizontal dipole axis;

iii. as the energy travels radially along the surface, a fraction of the energy continuously refracts into the sea; and this fraction of energy essentially travels directly downward as a rapidly (exponentially) attenuating uniform plane wave.

Summarizing, the path of propagation from a submerged transmitting dipole to an arbitrary receiving dipole in the sea is the following: From the transmitting dipole, directly up through the sea to the surface, through the air along the

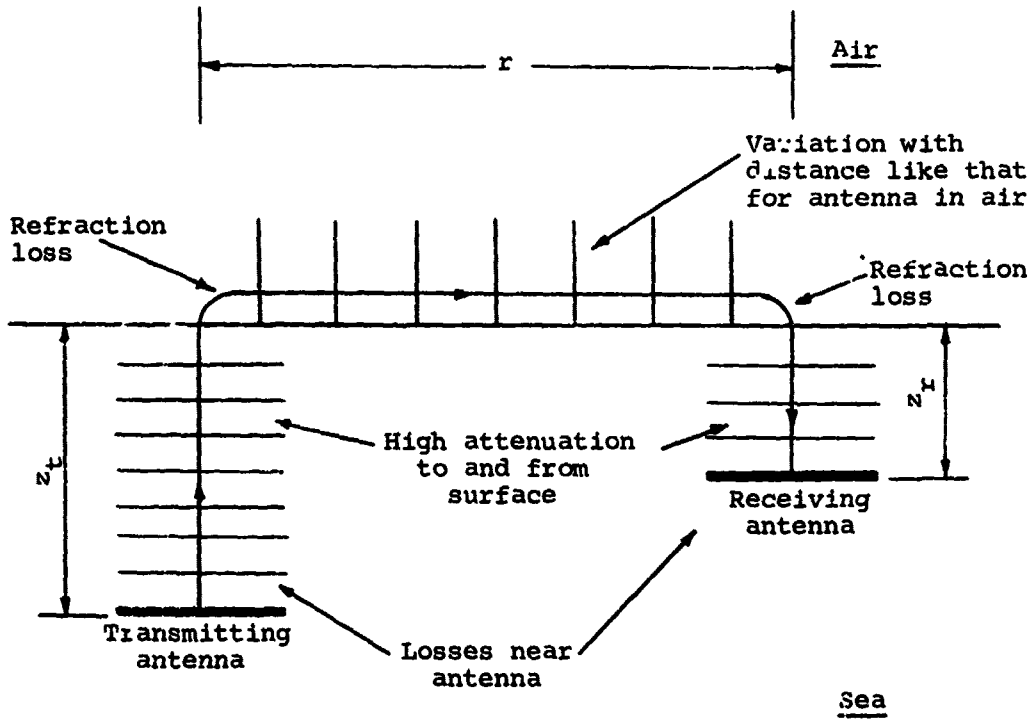


Figure 1--Path of propagation

surface, and directly down through the sea to the receiving dipole, as shown in Figure 1. The largest attenuation is incurred (1) as the wave travels through the sea and (2) as the wave refracts out of and back into the sea.

The field components in the sea [Moore and Blair, 1961; Baños and Wesley, 1953] for a submerged horizontal electric transmitting dipole are the following:

For near field:

$10^{-1} < \rho \leq 1$, $z_t \geq 0$, $z_r \geq 0$, $z \ll \rho$, $f < 50$ kc/s.

$$E_r \approx 5.92 \times 10^{-27} \frac{\omega^3 I\ell e^{-z/\delta}}{\sigma\rho^3} (1 + j\rho - \rho^2)\cos \phi \qquad (1)$$

$$E_\phi \approx 1.18 \times 10^{-26} \frac{\omega^3 I\ell e^{-z/\delta}}{\sigma\rho^3} (1 + j\rho)\sin \phi \qquad (2)$$

$$E_z \approx 0\left[\frac{\rho}{\sqrt{g}} (E_r \text{ or } E_\phi)\right], \text{ negligible.} \qquad (3)$$

$$H_\phi \approx -\sqrt{-j}\ 5.26 \times 10^{-24} \frac{\omega^{5/2} I\ell e^{-z/\delta}}{\sigma^{1/2}\rho^3}(1 + j\rho - \rho^2)\cos \phi = \frac{E_r}{\eta_1} \qquad (4)$$

$$H_r \approx \sqrt{-j}\ 1.05 \times 10^{-23} \frac{\omega^{5/2} I\ell e^{-z/\delta}}{\sigma^{1/2}\rho^3}(1 + j\rho)\sin \phi = -\frac{E_\phi}{\eta_1} \qquad (5)$$

$$H_z \approx 0\left[\frac{1}{\sqrt{g}\,\rho} (H_r \text{ or } H_\phi)\right], \text{ negligible} \qquad (6)$$

For far field:

$1 \leq \rho < 10^2$, $z_t \geq 0$, $z_r \geq 0$, $z \ll \rho$, $f < 50$ kc/s.

$$E_r \approx -5.92 \times 10^{-27} \frac{\omega^3 I\ell e^{-z/\delta}}{\sigma\rho} (1 - \frac{j}{\rho} - \frac{2}{\rho^2})\cos \phi \qquad (7)$$

$$E_\phi \approx j\ 1.18 \times 10^{-26} \frac{\omega^3 I\ell e^{-z/\delta}}{\sigma\rho^2} (1 - \frac{j}{2\rho})\sin \phi \qquad (8)$$

$$E_z \approx 0\left[\frac{1}{\sqrt{g}} (E_r \text{ or } E_\phi)\right], \text{ negligible} \qquad (9)$$

$$H_\phi \approx \sqrt{-j}\ 5.26 \times 10^{-24} \frac{\omega^{5/2} I\ell e^{-z/\delta}}{\sigma^{1/2}\rho} \left(1 + \frac{j}{\rho} - \frac{2}{\rho^2}\right) \cos\phi = \frac{E_r}{\eta_1} \quad (10)$$

$$H_r \approx -\sqrt{j}\ 1.05 \times 10^{-23} \frac{\omega^{5/2} I\ell e^{-z/\delta}}{\sigma^{1/2}\rho^2} \left(1 - \frac{j}{2\rho}\right) \sin\phi = -\frac{E_\phi}{\eta_1} \quad (11)$$

$$H_z \approx 0\left[\frac{1}{\sqrt{g}\,\rho} (H_\phi \text{ or } H_r)\right], \text{ negligible.} \quad (12)$$

For the field just at or slightly above the surface, the theory states the following:

For the near field:

$$10^{-1} < \rho \leq 1,\ z_t \geq 0,\ z_r = 0,\ z \ll \rho,\ f < 50 \text{ kc/s},$$

$$E_z \approx -\sqrt{j}\ 1.98 \times 10^{-21} \frac{\omega^{5/2} I\ell e^{-z_t/\delta}}{\sigma^{1/2}\rho} (1 + j\rho)\cos\phi \quad (13)$$

For the far field:

$$1 \leq \rho < 10^2,\ z_t \geq 0,\ z_r = 0,\ z \ll \rho,\ f < 50 \text{ kc/s},$$

$$E_z \approx -\sqrt{-j}\ 1.98 \times 10^{-21} \frac{\omega^{5/2} I\ell e^{-z_t/\delta}}{\sigma^{1/2}\rho^2} \left(1 - \frac{j}{\rho}\right)\cos\phi \quad (14)$$

All other field components in the air near the surface are negligible in magnitude compared to $E_z$.

The coordinate system is illustrated in Figure 2, and

$z_t$ is transmitting antenna depth

$z_r$ is receiving antenna depth

$z = z_t + z_r$, is vertical distance (downward) in cylindrical coordinate system

r is radial distance in cylindrical coordinate system

$\phi$ measured positive from x-axis

$\rho$, distance factor, $= \frac{\omega}{c} r = 2\pi r/\lambda_o$ .

$\zeta$, depth factor, $= \frac{\omega}{c} z = 2\pi z/\lambda_o$

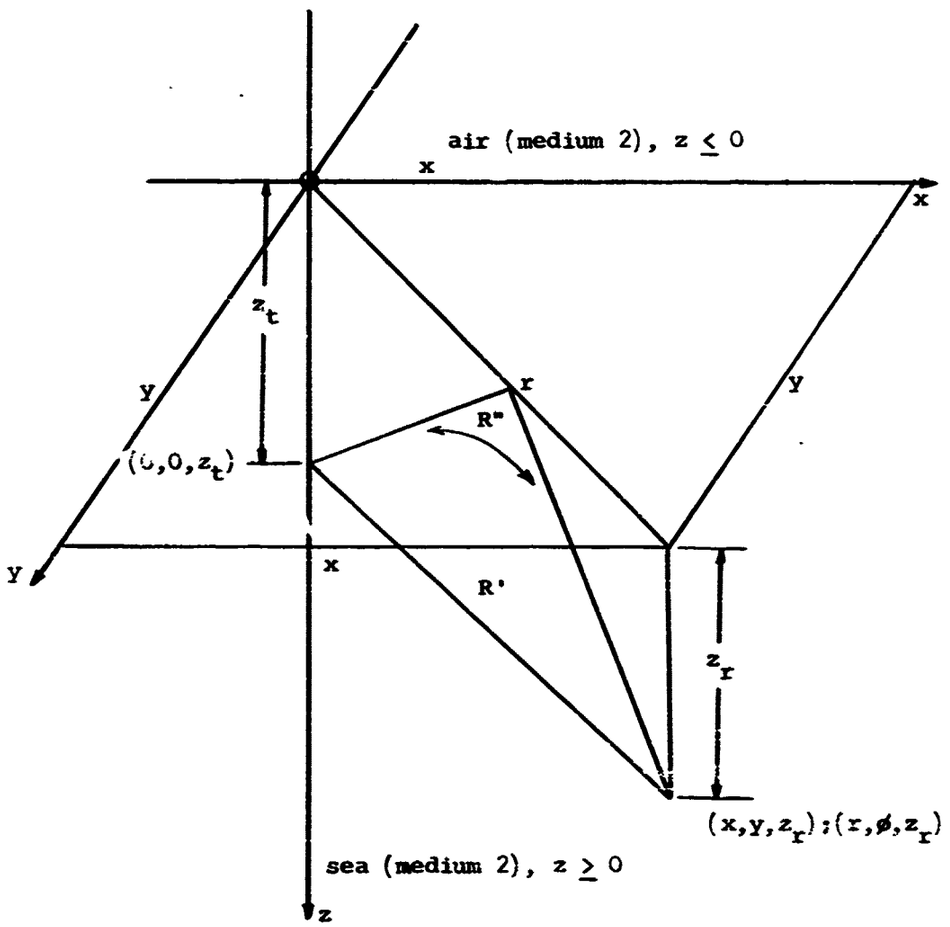


**Figure 2--Distances and coordinate system**

$\omega$, radian frequency = $2\pi f$; f, frequency in cps.

c is speed of light in free space

$\lambda_o$ is free-space-wavelength

$\delta$, skin depth = $\sqrt{2/\omega\mu_o\sigma_1}$

$\sigma_1$ is conductivity of sea $\approx$ 4 mhos/meter

$\mu_o$, $\epsilon_o$ are permeability and permittivity, respectively, of free space

$I\ell$ is antenna moment magnitude

I is r.m.s. antenna current (constant over length, $\ell$)

$\ell$ is antenna length

$g = \frac{\sigma}{\omega\epsilon_o} \approx |n^2|$ ; $\eta_1$, intrinsic impedance of sea = $\sqrt{j\omega\mu_o/\sigma_1}$

$n^2$ is the index of refraction of the sea with respect to free space

$i = \sqrt{-1}$ and only the first quadrant root of $\sqrt{j}$ and fourth quadrant root of $\sqrt{-j}$ are used.

Unrationalized MKS system of units is used.

## 3.0 Experimental Model for Verification of Theory

The modeling technique reported herein is premised on two facts: (1) Only electric fields need be measured; from the electric field, the magnetic fields can be determined. Similarly, if only magnetic fields are measured, then the electric fields can be determined. However, for most of the experimental work here, the electric field components were measured. (2) Frequency and conductivity scaling is such that a laboratory scale experiment can be used (that is, a tank several feet in diameter with antennas a few inches long).

Modeling at this small scale has the usual advantages of a laboratory-size model such that (1) one or two technicians

can easily operate the model; (2) antenna position for depth, orientation, separation between antennas, can be adjusted quickly and conveniently; (3) because the frequencies are higher, antenna impedances are higher, thus matching difficulties can be more easily eliminated; (4) various control conditions and uniformity can be obtained (for example, the conductivity of the conducting medium, salt water, can be changed easily; (5) materials and equipment costs are considerably reduced from those of larger models.

3.1 Scaling Ratios for Model. This modeling technique actually employs wavelength scaling, not similitude scaling. In a dielectric medium, the wavelength scaling factor, $S_2$, is expressed as follows:

$$S_2 \sim \lambda_2 \sim f^{-1} , \quad \text{here } \lambda_2 = \lambda_o . \tag{15}$$

A conducting medium is specified by a complex permittivity, $\underline{\varepsilon}$,

$$\underline{\varepsilon} = \varepsilon - j\sigma/\omega \tag{16}$$

such that $\sigma/\omega >> \varepsilon$. This inequality means that for a given $\sigma$ and $\varepsilon$ of a conducting medium, then $f << \sigma/2\pi\varepsilon$. The scaling factor, $S_1$, in the sea is then expressed as follows:

$$S_1 \sim \lambda_1 = 2\pi\delta \sim (\sigma f)^{-1/2} \tag{17}$$

Thus for wavelength scaling, the air (dielectric) scaling factor, $S_2$, varies as $f^{-1}$; and the salt water (conductor) scaling factor, $S_1$, varies as $(\sigma f)^{-1/2}$, for $f << 900$ mc/s. In actual practice, it was determined that if $f \leq 400$ mc/s, the medium still maintained satisfactory characteristics as a conducting medium.

Wavelength, or frequency, scaling provides two useful experimental advantages: (1) because of the available wide range of frequencies, one can obtain very large scaling factors. (2) Moreover, the scaling factor is different in the salt water in the tank than in the air above the tank. This has the advantage that if a distance in air is scaled by $10^{-4}$, then a distance in the sea, or salt solution, is scaled by only $10^{-2}$. For example, using these scaling factors, an air distance of 10 km. is scaled to 1 meter; but a 10 m. antenna in the sea is scaled to 10 cm, which is convenient laboratory size for a model antenna. For this reason, similitude scaling is undesirable, since the 10 m. antenna would also be scaled by $10^{-4}$ down to 1 mm., which is an inconveniently small laboratory size.

Consequently, the scaling factors are determined for both air and tank solution as follows:

for air, the scaling factor $S_2 = \frac{f}{f_m}$

for conducting medium, the scaling factor $S_1 = \left(\frac{f\sigma_1}{f_m \sigma_{1m}}\right)^{1/2}$

where $f_m$ = model frequency

$f$ = original frequency

$\sigma_{1m}$ = conductivity of model tank solution

$\sigma_1$ = original conductivity of sea.

For example:

| Parameters | Actual Values | Model Values |
|---|---|---|
| frequency, f, c/s | $10^4$ | $10^8$ |
| conductivity, $\sigma$, mhos/meter | 4 | 16 |
| ($\therefore$ scale factors are $S_2 = 10^{-4}$, $S_1 = 5 \times 10^{-3}$) | | |
| skin depth, $\delta$, | 2.5 m. | 0.25 m. |
| separation, d, | 20 km. | 2 m. |
| antenna length, $\ell$, | 20 m. | 10 cm. |
| transmitting antenna depth, $z_t$ | 20 m. | 10 cm. |
| receiving antenna depth, $z_r$ | 30 m. | 15 cm. |

The impedance of a horizontal electric dipole; that is, a coaxial transmission-line type antenna, submerged in a conducting medium [Flath, 1949; Moore, 1951] is:

$$Z = \frac{\omega\mu_1\ell}{8} + j\frac{\omega\mu_1\ell}{2\pi}\left[0.116 + \ln(a\sqrt{2})\right], \; 0 < \delta b \ll 1, \; \frac{b}{a} > 2, \; b \ll \lambda_3 \quad (18)$$

where a = diameter of inner conductor of coaxial antenna.

b = diameter of dielectric of coaxial antenna.

$\lambda_3$ = wavelength in dielectric

The outer conductor is actually the sea of conducting salt-water solution surrounding the dielectric. This is discussed in detail later. It is interesting to realize that the resistance is independent of the diameters of the inner conductor and dielectric as well as the conductivity of the sea or tank solution. Moreover, the reactance is a function of inner conductor diameter, a, only, and is independent of the dielectric diameter, b. Thus as long as $(b/a) > 2$, $b \ll \lambda_3$, the impedance is independent of b. Continuing the above example:

| Parameters | Actual Values | Model Values |
|---|---|---|
| a, | 2.0 cm. | 0.10 mm. |
| b, | 5.0 cm. | 0.25 mm. |
| $Z$ | 1.97 - j 0.62 ohms | 99 - j 127 ohms |

The model values for a and b appear to be quite small, but the ratio (b/a) = 2.5 can be increased considerably without changing the impedance or violating any theoretical restrictions. Actually larger model values of a and b are used for the experimental work (see Appendix), and this has no effect on the use of the modeling technique nor on the experimental verification of the theory used here.

3.2 Experimental Model and System. The cylindrical tank filled with salt water used in this model is shown in Figure 3. A wooden frame supports a wooden crossbeam over the tank. The submerged transmitting and receiving antennas are mounted on the end of the vertical plastic rods which are attached to the two slide blocks on the crossbeam. Each slide block is conveniently positioned along the crossbeam by a nylon cord and pulley arrangement which is fastened onto the top of the crossbeam. The signal generator, driving the transmitting antenna, is shown to the right of the tank on the floor. Similarly, the receiving equipment is shown to the left of the tank.

The slide block, antenna rod, and coaxial antenna are shown in Figure 4. The slide blocks are made entirely of plastic so that the wooden beam and plastic slide block combination produce negligible distortion of the electromagnetic fields on and just above the surface of the tank.

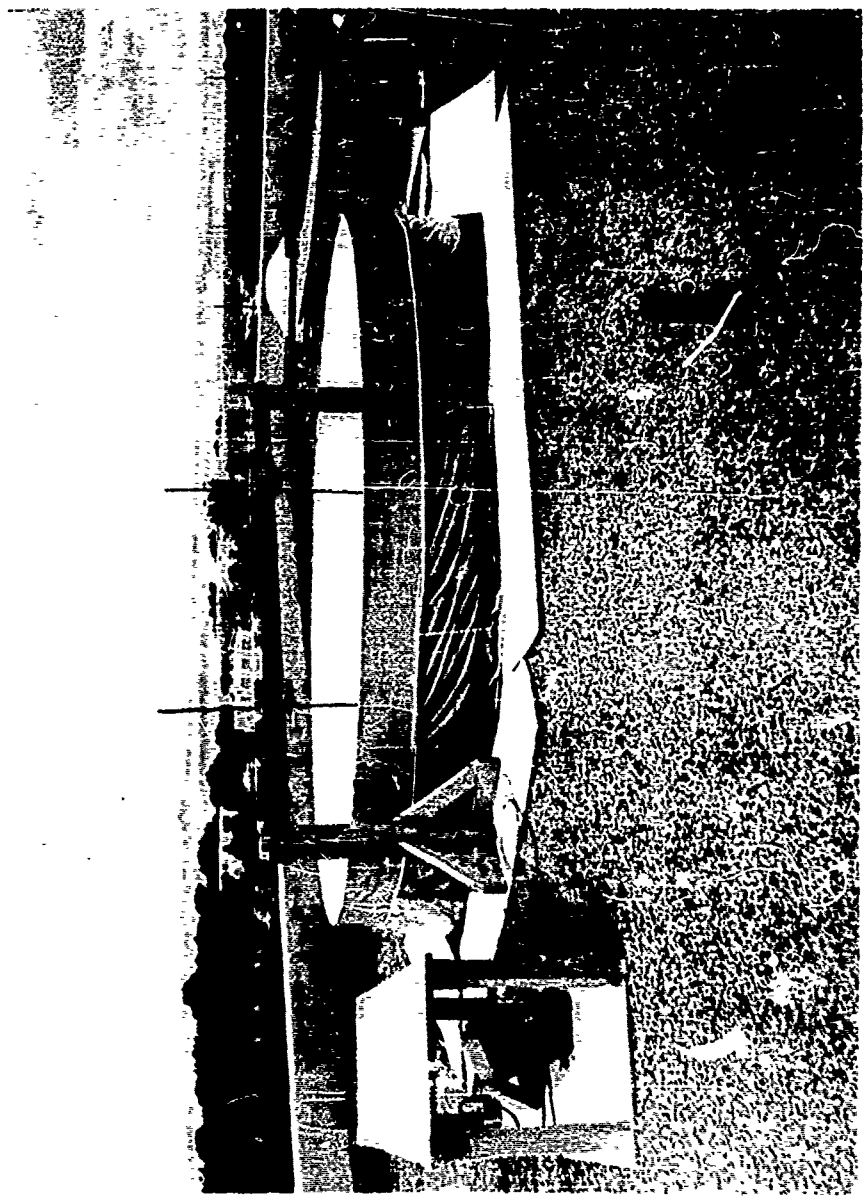

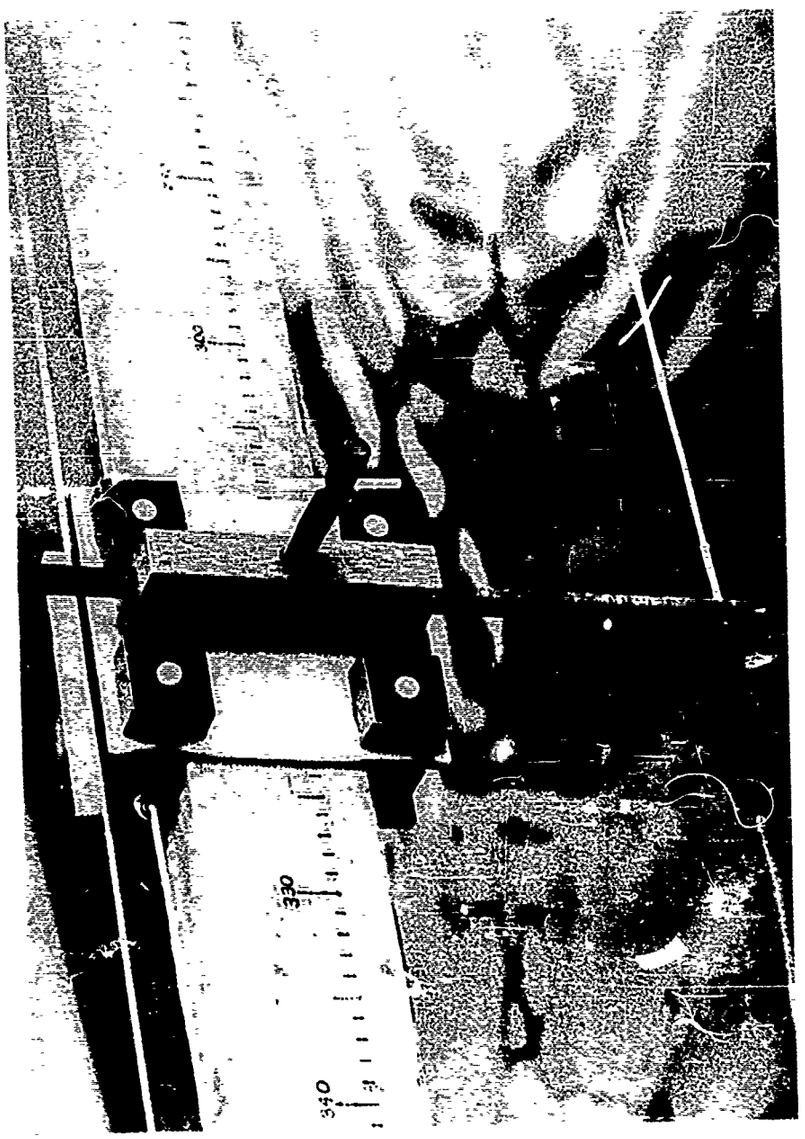


Figure 4--Slide block and antenna mount

Centimeter marks on the beam and the rod are for horizontal and vertical positioning of the antennas.

The coaxial antenna used as a horizontal electric dipole is shown in Figure 5. This is essentially a short-circuited coaxial (transmission-line) antenna that is made as follows (see Figure 6): (1) The insulation, outer conductor, and dielectric are stripped back from an open end of the coaxial cable, exposing the inner conductor to the salt water. The length of the exposed inner conductor must be at least $\lambda_1/4$, where $\lambda_1$ is the wavelength in the sea. (2) Then the insulation and outer conductor are stripped back exposing the dielectric for a length, $\ell$, where $\ell$ is the dipole length. The length, $\ell$, must be less than $\lambda_3/4$, where $\lambda_3$ is the wavelength in dielectric. (3) Finally the insulation is stripped at least one centimeter, exposing the outer conductor. The antenna is shown mounted in the end of the vertical plastic rod.

The nature of this coaxial antenna can be described [Moore, 1951] as follows: The phase velocity of a wave traveling through the dielectric for $2 < (b/a) < 10$, where $b/a$ is the ratio of dielectric diameter to inner conductor diameter, is in the order of half that of the velocity of light. Consequently, for the frequencies used in this modeling technique, $\ell << \lambda_3/4$. It is then rather obvious that the r.m.s. current, I, through the inner conductor over the exposed length, $\ell$, is nearly constant. Furthermore, the current is conducted from the exposed inner conductor through

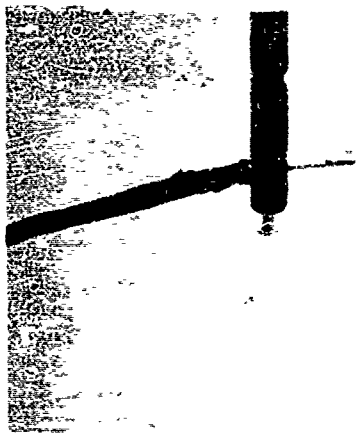

Figure 5--Model coaxial antenna

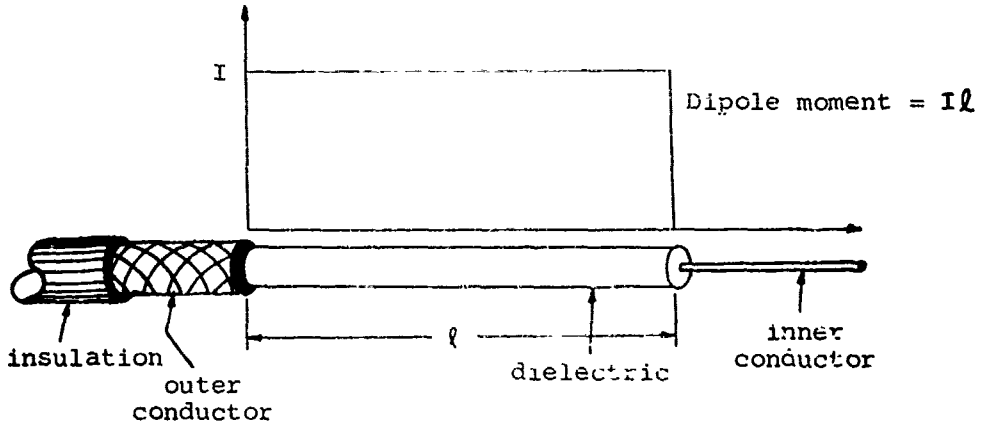


(a) Short-circuited dipole

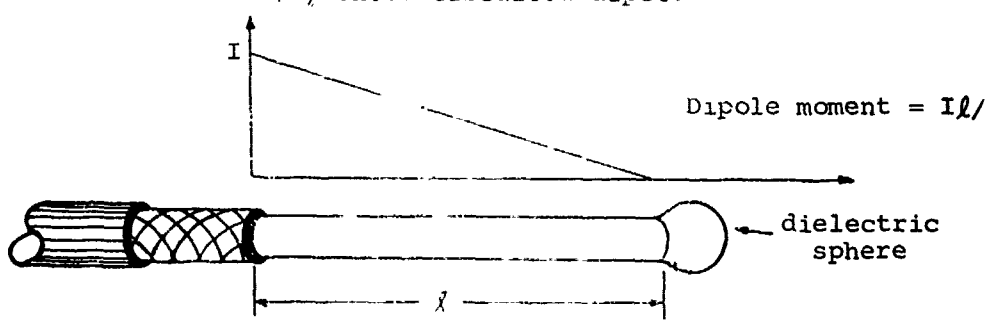


(b) Open-circuited dipole

the sea to the exposed outer conductor. Because I is nearly constant, the dipole moment Iℓ, as shown in Figure 6a, is constant.

A variation of this antenna is the open-circuited coaxial (transmission-line) antenna, which is the same as the short-circuit antenna except that the inner conductor is cut off at the end of the dielectric and the inner conductor is insulated from the sea. Since the current at the end of the open circuit antenna is zero, the current decreases approximately linearly from I at the beginning of the antenna to 0 at the end of the antenna. Consequently, the dipole moment is Iℓ/2, as shown in Figure 6b.

The model tank, transmitting and receiving equipment, and apparatus were placed on a University of New Mexico dormitory roof. Figure 7 is a telephoto of the setup showing the receiving antenna being adjusted. The tank had to be placed so that any object above the surface of the tank had negligible reflection coefficient or was several wavelengths away, in order to prevent reflections from distorting the field patterns over the surface of the salt water in the tank. Since an anechoic chamber was not available, the setup was placed on the roof where the nearest obstacle higher than the surface of the water was the dormitory penthouse 100' from the tank (usually 5 to 50 wavelengths from the tank).

When a remote meter was used to indicate the field strength, the data taker was at least 20' from the tank. Consequently, there was no metal or material with significantly large

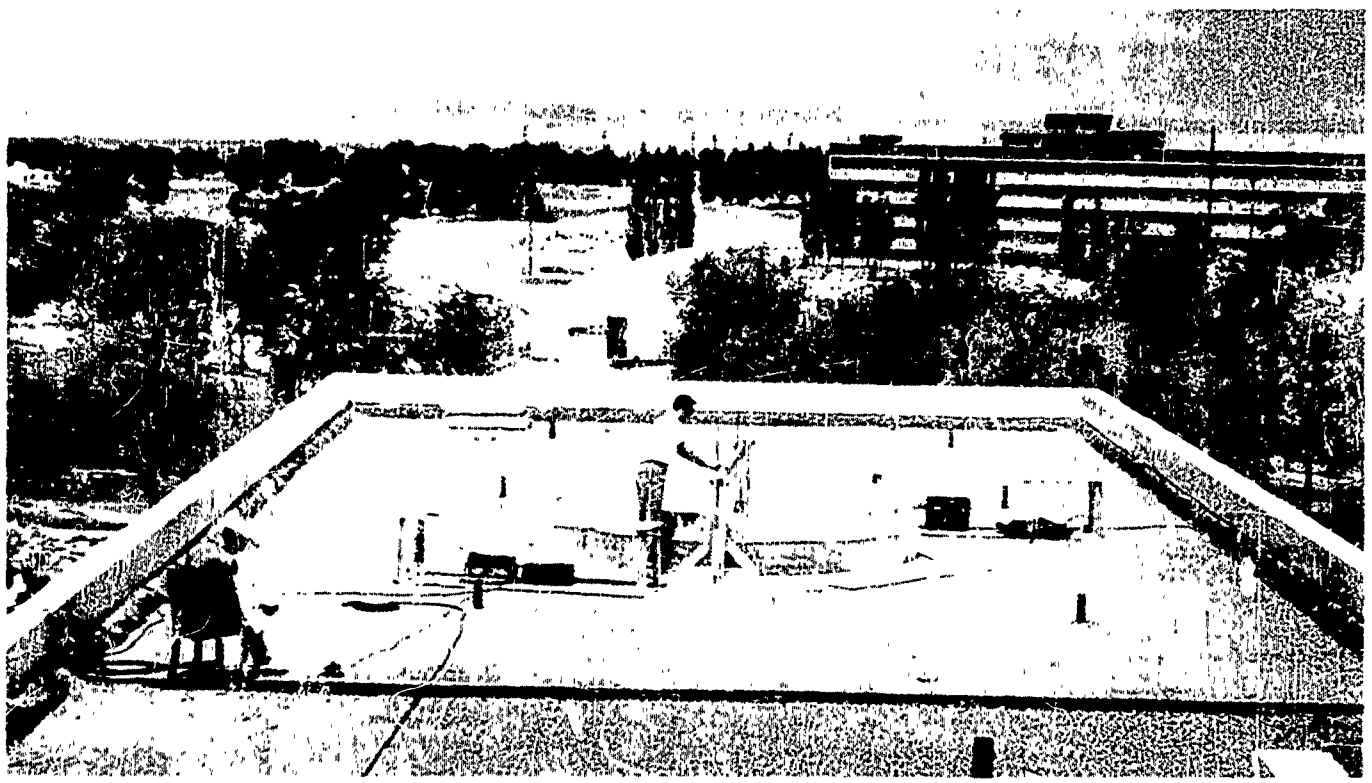

Figure 7. Field measurements using model tank

reflection coefficient above the surface of the tank for a radius of over 100'.

A detailed list of materials and specifications of the model tank and apparatus is given in the Appendix.

## 4.0 Experimental Measurements and Results

4.1 Field Components Measured in the Sea. The horizontal electric dipole is used as a transmitting antenna because it is the most efficient radiator in the sea and the theory describing the radiation fields from this dipole is well known. The following Figures 8 through 15 show the comparison with various parameters of experimental to theoretical results for variation of $E_r$ and $E_\phi$ electric field components in the salt water model sea. The important parameters that are used as independent variables are: separation between antennas, $\rho$; antenna depth, z; relative angular orientation $\phi$; antenna length, $\ell$; and antenna current, I.

Figure 8. One common problem with a finite model of the earth, used for radiation measurements, is to eliminate all extraneous reflections from the finite boundaries of the model, thus eliminating standing waves in the region of measurement. One convenient method of determining the standing wave pattern on the surface of the salt water in the tank is to fix the separation between the transmitting and receiving horizontal elelctric dipoles and then move the dipoles along the diameter without changing antenna separation, depth or orientation. If there is no standing surface wave, the detector should show a constant field strength, regardless of the position of the

dipoles in the tank. If the transmitting dipole has an input voltage in the order of a volt and the receiving dipole is separated far enough to measure a few microvolts, this test is sufficiently sensitive to check for a standing surface wave. Figure 8 shows the field strength deviation from the mean to be less than one microvolt for all situations tested. For the various frequencies used, the deviation is plotted as a function of the distance from the edge of the tank to the midpoint between transmitting and receiving antennas.

If either dipole were positioned a distance less than about two wavelengths in salt water from the side of the tank, then the reflections are sufficiently large to cause incorrect field-strength data. Consequently, the transmitting and receiving dipoles were always kept far enough from the edge of the tank so that there were negligible reflections from the side and edge of the tank.

Figure 9. A critical test of this modeling system is the comparison of the absolute value of the experimental to theoretical electric field components for a given set of variables. Figure 9 shows a comparison of the $E_r$ and $E_\phi$ field components (1), (2), (7), (8), in the sea as a function of radial distance factor, $\rho = 2\pi r/\lambda_o$, thus checking both near-zone fields ($\rho \leq 1$) and far-zone fields ($\rho \geq 1$). Theoretically, the slope to a first order approximation is -3 in the near-zone; and is -1 for the $E_r$ component and -2 for the $E_\rho$ component in the far-zone. Consequently, the division between the near-zone and the far-zone ($\rho = 1$), common to both the near-zone and far-zone components, appears to have a discontinuous slope. This never occurs in nature and a second order theory expanded

about $\rho = 1$ indicates [Moore, 1951; Banos, 1954; 1954] that the slope has continuous derivatives.

The theory is restricted to the case of $r >> z$. It is interesting to note this indicates that the theoretical restrictions are more conservative than they need by; because if the experimental data is compared to the theoretical data for $r \geq 2.5\ z$ and $r \geq 2.5\ \ell$, then theory and experiment agree remarkably well.

The experimental $E_r$ curve diverges upward from the theoretical curve with decreasing separation between the two antennas; the reason is (effectively) that the receiving antenna is moved too close to the transmitting antenna so that the receiving antenna no longer "sees" the transmitting antenna as a point source. The experimental field components diverge upward from the theoretical curves with increasing separation between antennas because the field intensity decreases to the noise level of the receiver.

Figure 10, 11. By varying the frequency of the transmitter, one can model various regions of the near-zone and far-zone fields. Figure 10 shows the variation of $E_r$ field component with distance factor for frequencies varying from 20 mc/s to 400 mc/s. Figure 11 shows the same results for $E_\phi$ field component. In both figures, the experimental curves diverge upward from the theoretical curve at both ends of the curves. The reasons are the same as those for Figure 9; that is, (1) as the separation decreases between the transmitting and receiving antennas, the receiving antenna no longer "sees" the transmitting as a point source; (2) as the separation

increases between the antennas, the field intensity decreases to the noise level, which is a constant with increasing separation.

Figure 12. Examination of (1) through (12) shows that all field components vary with total depth, z, as $\exp(-z/\delta)$. Figure 12 compares the experimental to theoretical variations of field intensity with z. When the field components are plotted on a semi-log graph, the field components theoretically vary linearly with a slope of $-1/\delta$. The curves diverge upward from the theoretical curve with decreasing field strength because the field intensity was approaching the noise level. Since the slope is a function of $\delta$, which is a function of $\sigma$, then this is also an indirect check on the exponential variation of $\sigma$.

Figure 13. As shown in Figure 12, the field components vary exponentially with the total depth, $z = z_t + z_r$; that is, the field components depend only on the sum of the depths of the transmitting dipole and the receiving dipole and do not depend on the relative depth of the dipoles. Figure 13 shows that if z is constant, the field components are independent of the relative $z_t$ and $z_r$. The abscissa shows various combinations of $z_t$ and $z_r$ such that $z = z_t + z_r$ is held constant. All other parameters are also held constant. The ordinate shows the deviation from the mean of the magnitude of the $E_r$ and $E_\phi$ field components. This deviation indicates a random variation of less than one micro-volt and represents a variation of field strength of less than 5%.

Figure 14. Examination of (1) through (12) shows that all field components vary with the polar angle, $\phi$, as cos $\phi$ or sin $\phi$, where $\phi$ is measured from the axis of the horizontal electric transmitting dipole. Specifically, the $E_r$ component (1) or (7) varies as cos $\phi$, and the $E_\phi$ component (2) or (8), as sin $\phi$. Since the variations are identical in all four quadrants, only the first quadrant variations are shown. Theoretically these cos $\phi$ or sin $\phi$ variations are semicircles, whose diameters are the maximum magnitude of each field component; both theoretical and experimental data have beer normalized by the maximum magnitude of the theoretical $E_r$ or $E_\phi$ component as the case may be.

The deviation of the experimental curve from the theoretical curve is caused by the situation that the receiving antenna did not "see" the transmitting antenna as a point source. Instead as the relative orientation between the two horizontal antennas changes, then the effective distance between the two antennas also changed; hence, the distance factor, $\rho$ , changed slightly with the variations in $\phi$. This deviation could be eliminated by using increased transmitting power and wider separation between antennas.

Figure 15. All field components (1) through (12) theoretically vary linearly with the transmitting electric dipole moment, $M = I\ell$. For a finite electric transmitting antenna, this means that the antenna be proportional to the dielectric length, $\ell$ , and to the uniform transmitting antenna current, I, such that $I\ell = M$. Figure 15 shows that the $E_r$ component varies linearly with I and $\ell$. The variation of $E_r$ with $\ell$ is

not as smooth as it should be, because the driving-point impedance (13) of the antenna is a function of length. Consequently, the impedance as well as the radiated field changes with length. This changing mismatch of the antenna to the transmitter was impossible to eliminate. In spite of this difficulty, Figure 15 still indicates that the $E_r$ component varies linearly with $\ell$. All other field components measured varied with I and $\ell$ in a similar manner.

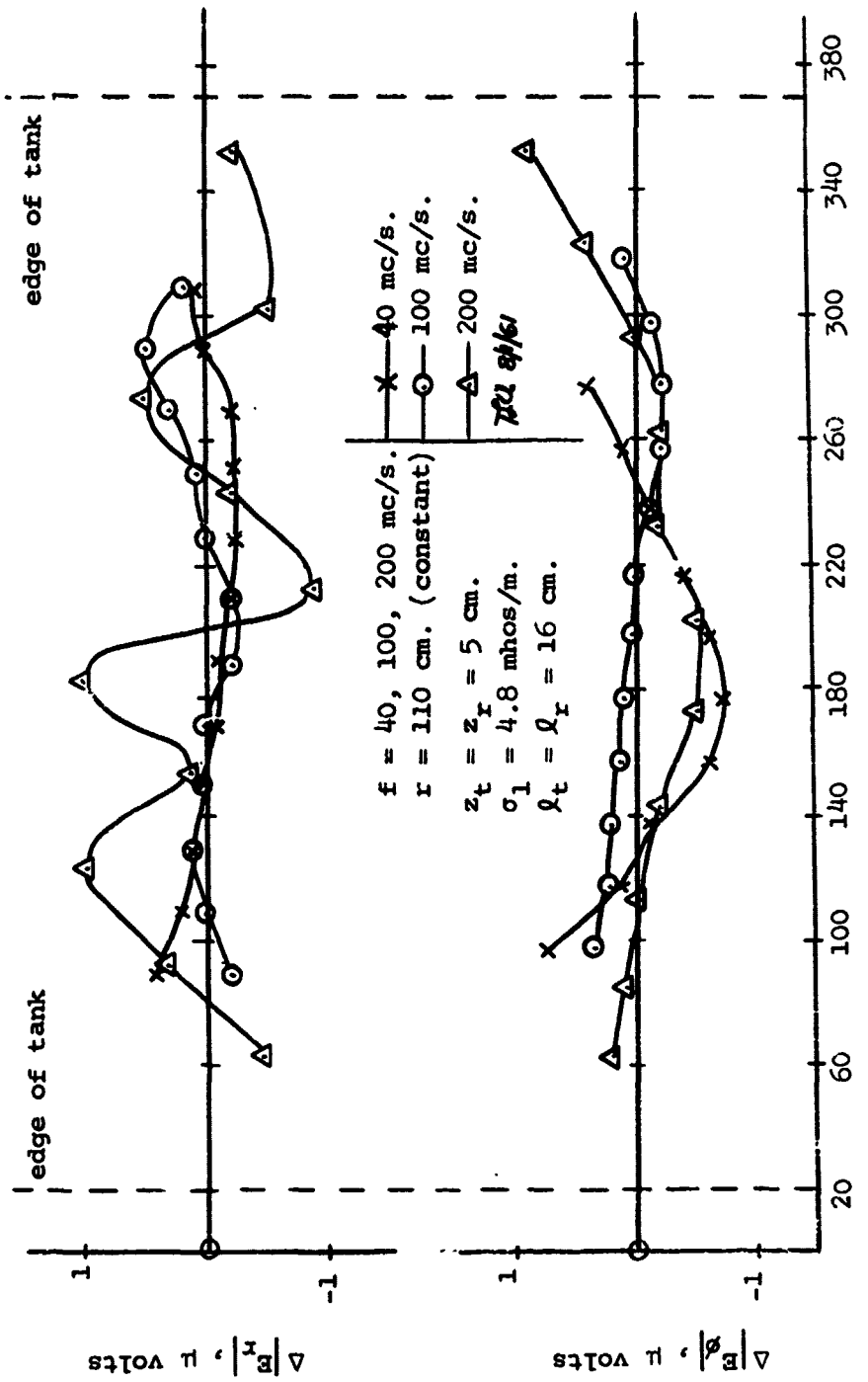


Figure 8--Testing for reflections on surface of salt water in model tank

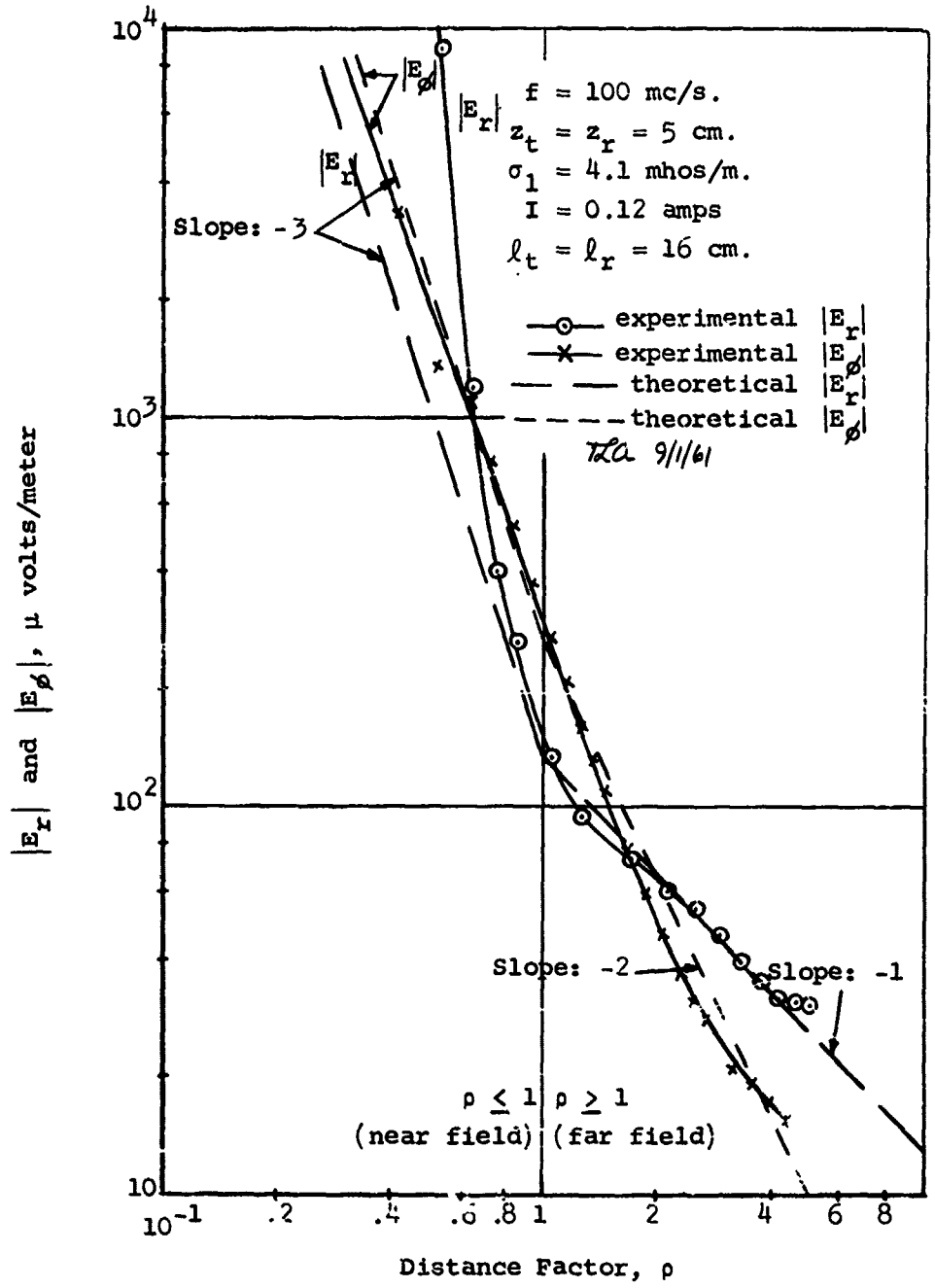


Figure 9--Variation of maximum magnitude of the electric field components with radial distance in units of free-space-wavelength/2π

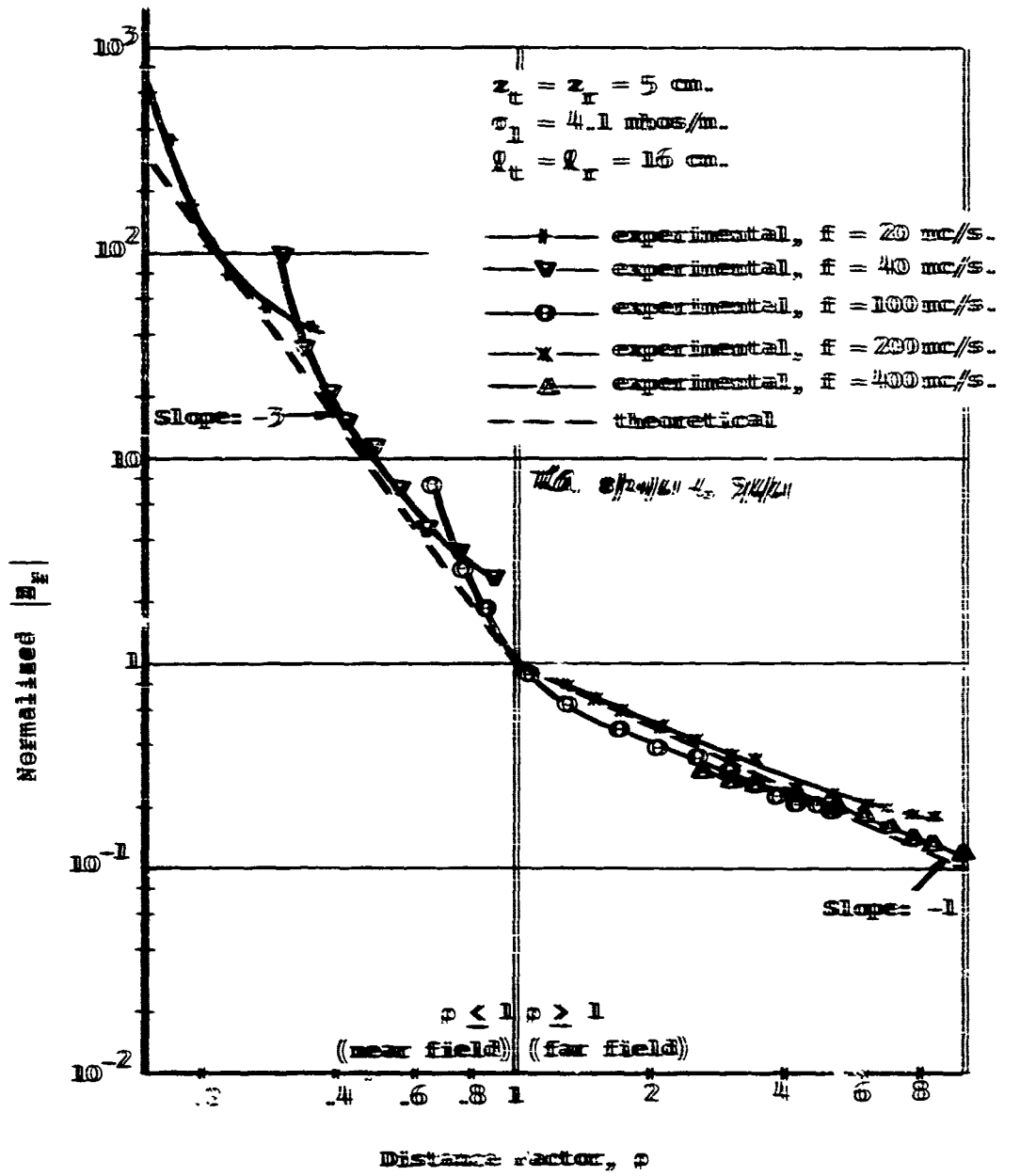


Figure 10—Variation of normalized magnitude of the electric field component, $E_r$, with radial distance in units of free-space-wavelength/$2\pi$.

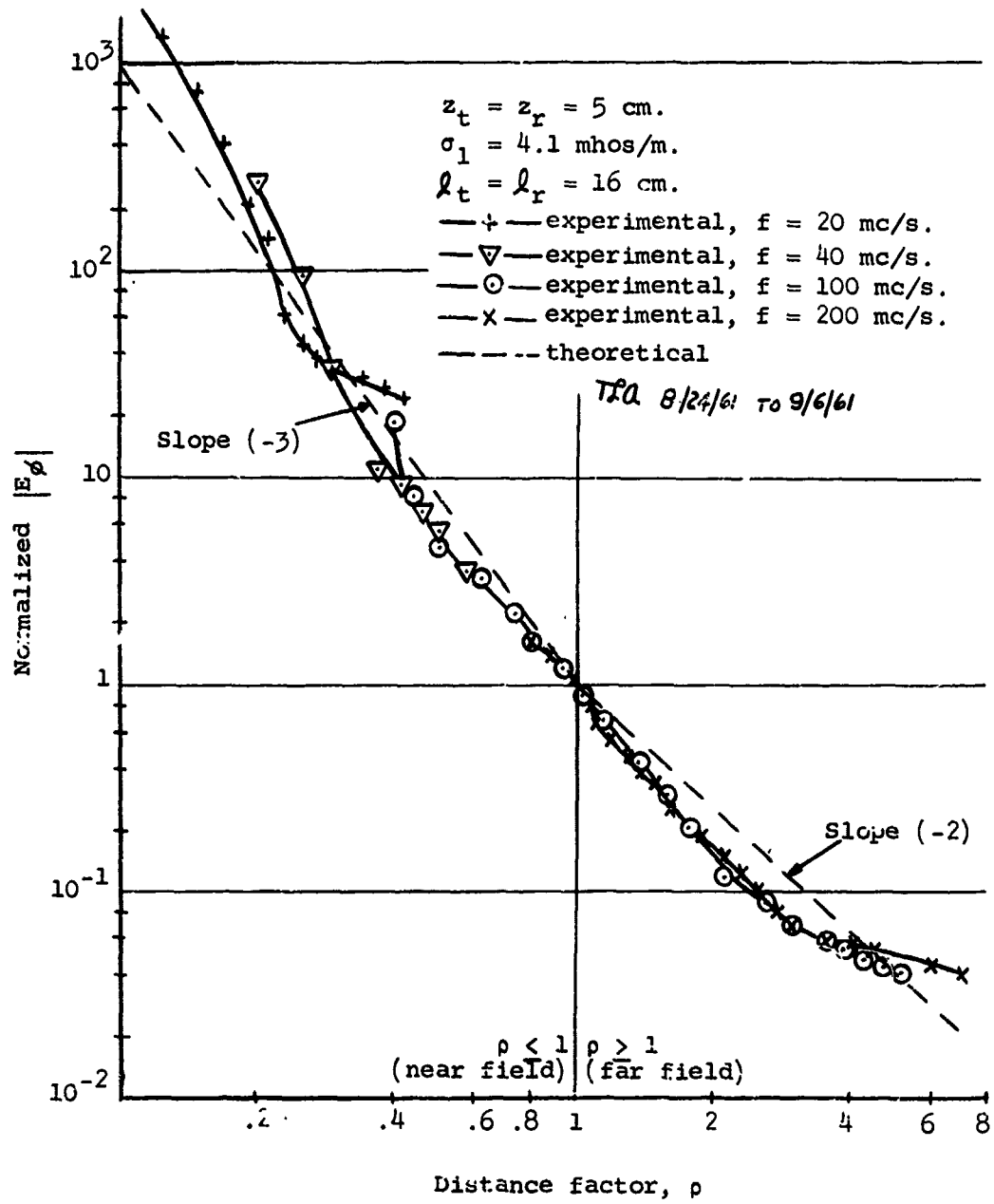


Figure 11--Variation of normalized magnitude of the electric field component, $E_\phi$, with radial distance in units of free-space-wavelength/$2\pi$.

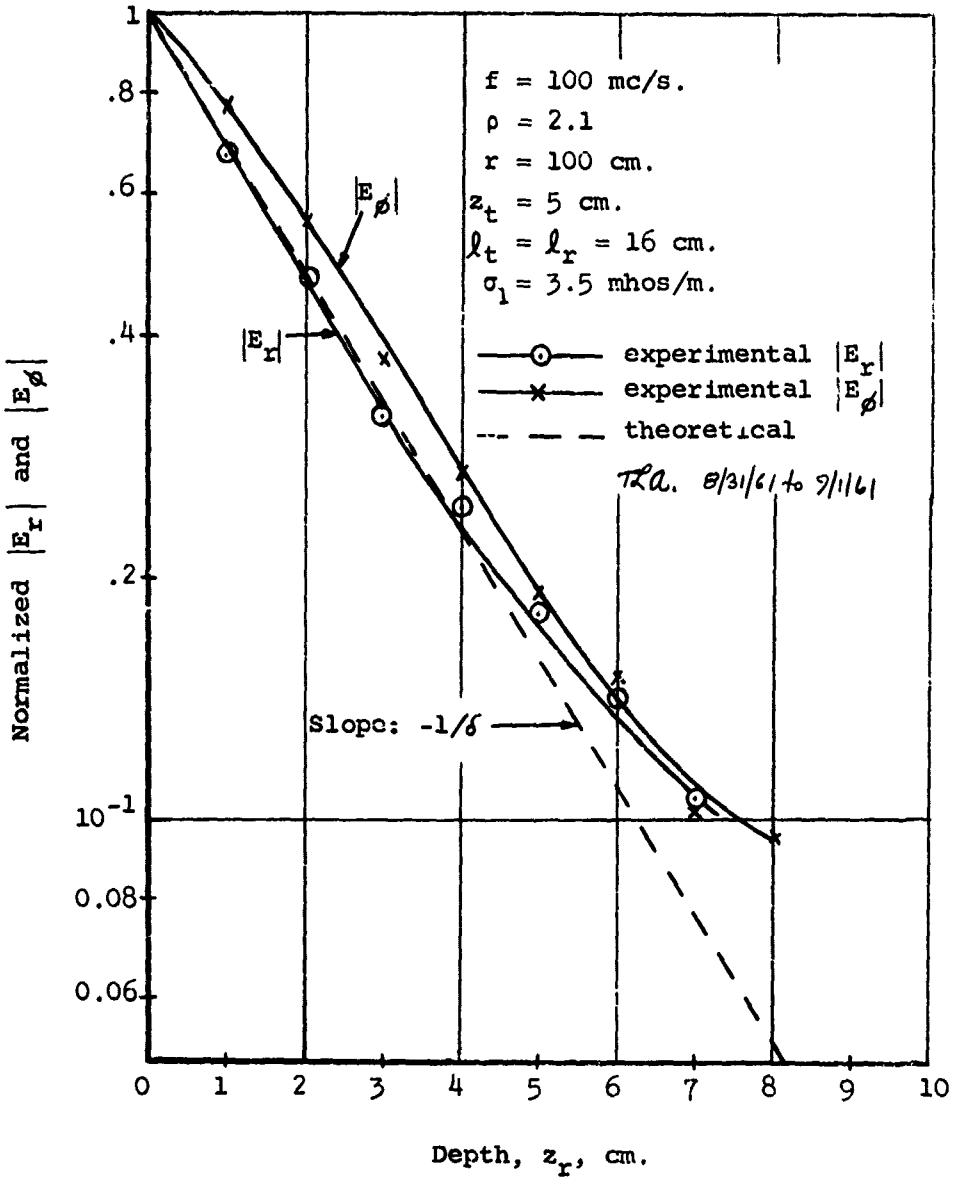


Figure 12--Variation of normalized maximum magnitude of the electric field components with depth

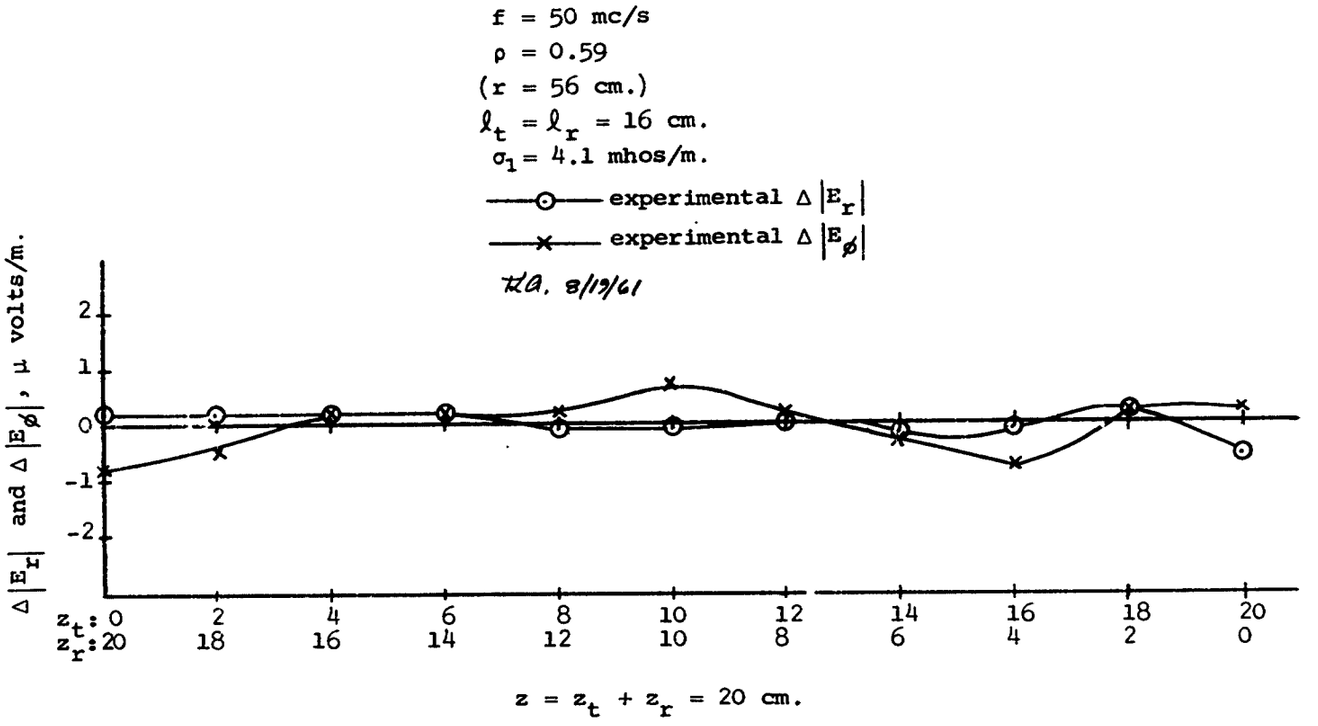


Figure 13--Deviation from the mean of the maximum magnitude of the electric field components with total depth of transmitting and receiving antennas constant

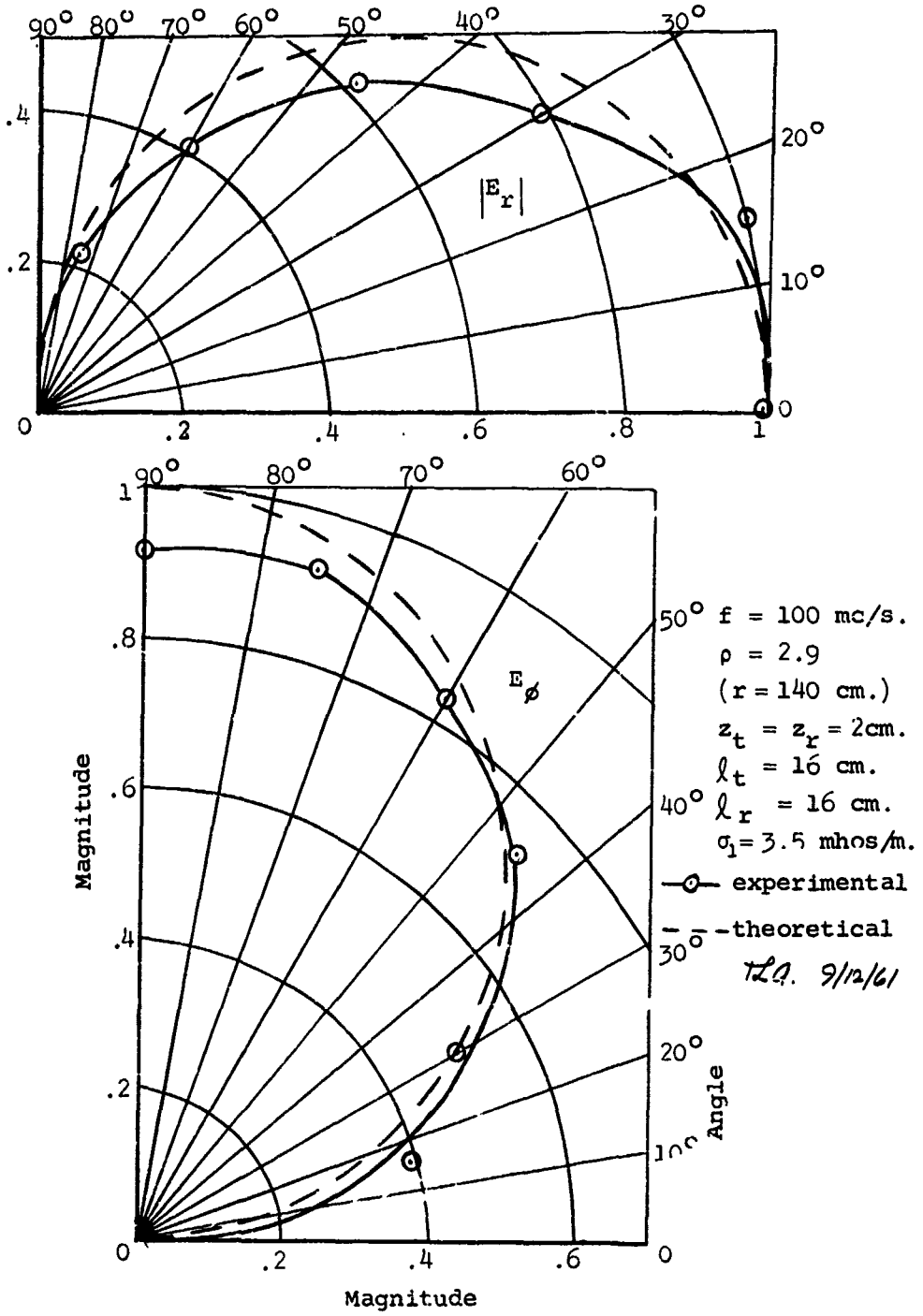


Figure 14--Variation of normalized magnitude of the electric field components with polar angle ø measured from horizontal electric dipole axis.

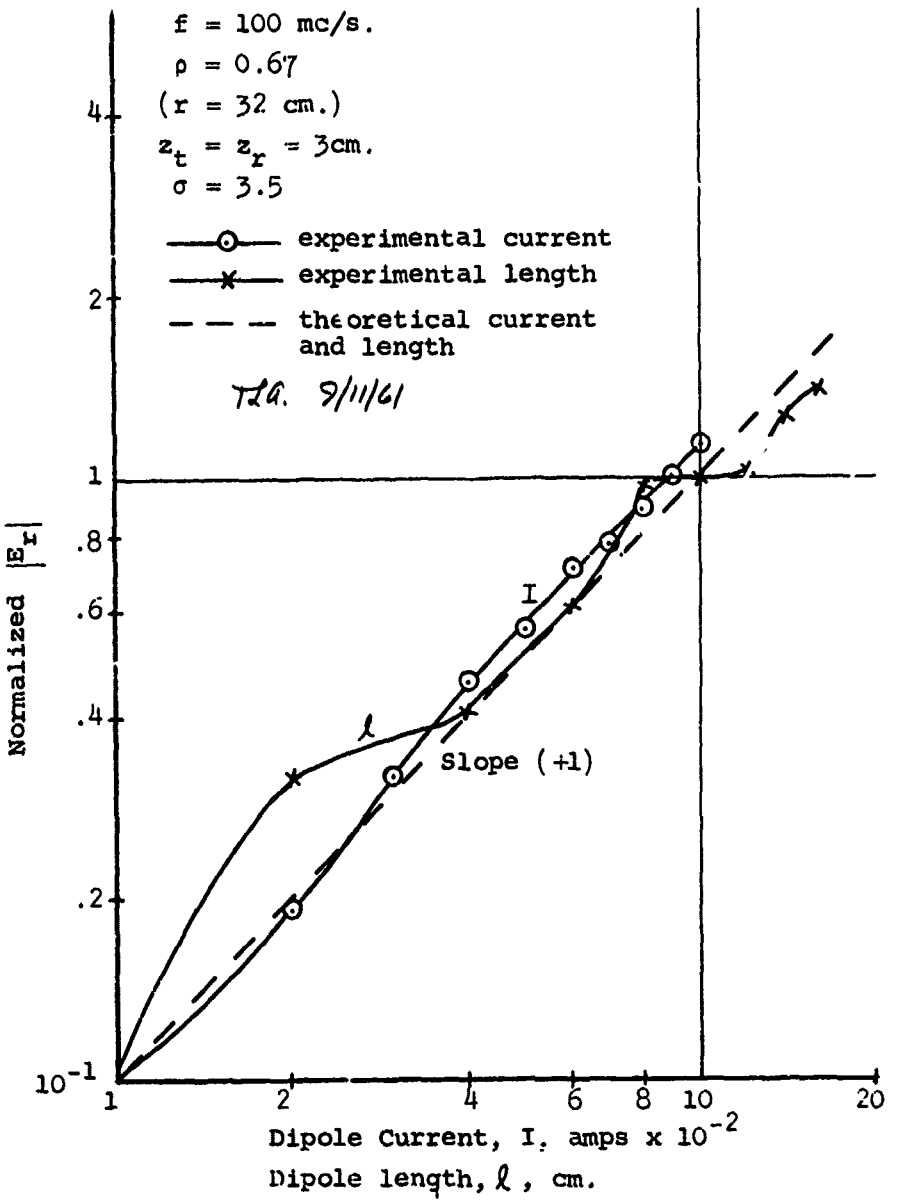


Figure 15--Variation of normalized magnitude of the electric field components with dipole current and length

4.2 Field Components Measured in Air. In addition to the $E_r$ and $E_\phi$ components measured in the salt water model sea, the $E_z$, $H_\phi$, and $H_r$ components were measured in the air over the surface of the sea. These components were measured as a function of $\rho \geq 0$ with all other parameters fixed, including fixed height, $-z_r$. Thus the receiving antenna passed directly over the transmitting antenna giving data in the static-zone, near-zone, and far-zone.

Theoretically there is no difference in the measurement technique between using the receiving antenna in the air or in the sea. However, there is one practical difficulty involving the field measurements in air: Any receiving antenna must be coupled through a transmission line to the field intensity meter, hence the transmission line distorts the field in the region near the receiver. This difficulty is avoided when the receiving antenna is submerged because the transmission line is also submerged; and since the wavelength in the sea is much shorter than the wavelength in air, there is negligible distortion of the received signal.

Figure 16. The $E_z$ component in air was measured by attaching a 16 cm. wire (electric monopole) to the vertical plastic rod on the slide blocks (see Figure 4). The slide block and antenna were kept at a constant height above the surface and were then moved radially outward ($\phi = 0$) from a point directly over the transmitting antenna ($r = 0$). Since the field in the static-zone was also measured, the theory for the normalized $E_z$ component is given [Baños, 1953]:

$$\left|E_z\right|_n = 2(5/4)^{5/2} \frac{z'r}{(r^2 + z'^2)^{5/2}}, \quad 0 \leq r << \lambda \qquad (19)$$

where the subscript n implies normalization such that

$\left|E_z\right|_{n\ \text{maximum}} = 1$ at $r = z'/2$ ,

$z' = z_t - z_r$, $z_r < 0$ since $z_r$ is above the surface (see Figure 2).

Baños has also shown that for the receiver height used in this model case, the $E_z$ component, which is the dominant field component, varies as $\rho^{-2}$ in the near-zone and $\rho^{-1}$ in the far-zone. This is predictable from the expressions for $E_z$ at the surface, (13) and (14).

Figure 16 shows the experimental data of $E_z$ as a function of $\rho$ compared to the three theoretical expressions for $E_z$ for the static-zone, near-zone, and far-zone. In spite of the distortion of the field by the receiving antenna transmission line, there is still reasonable agreement between experimental and theoretical data. It is interesting to note that the theories for the static-zone and the near-zone do not overlap in the ranges of validity.

Figures 17, 18. The $H_\phi$ and $H_r$ components in air were measured by attaching a 3" diameter loop to the vertical plastic rod at a fixed height on the slide block. The axis of the loop was oriented perpendicular and parallel to the transmitting antenna axis for measurement of $H_\phi$ and $H_r$ components, respectively. The $H_\phi$ and $H_r$ components were measured as a function of r with $\phi = 0$, for $r \geq 0$. Consequently, these two magnetic field components were measured as r varied from the static-zone

through the near-zone to the far-zone. The theory for the normalized $H_\phi$ and $H_r$ components [Baños, 1953] are:

$$|H_\phi|_n = 2\left(\frac{z'}{r}\right)^2\left[1 - \frac{z'}{(r^2 + z'^2)^{1/2}}\right] \quad (20)$$

$$|H_r|_n = 2\left(\frac{z'}{r}\right)^2\left\{\frac{z'r}{(r^2 + z'^2)^{3/2}} - \left[1 - \frac{z'}{(r^2 + z'^2)^{1/2}}\right]\right\} \quad (21)$$

where $|H_\phi|_{n\ \text{maximum}} = 1$ at $r = 0$.

Baños has also shown that for the receiver height used in this model case, the $H_\phi$ and $H_r$ components vary as $\rho^{-3}$ in the near-zone and vary as $\rho^{-1}$ and $\rho^{-2}$, respectively, in the far-zone. Since the tangential magnetic field components are continuous across the surface boundary, these $\rho$ variations are predictable from the expressions for $H_\phi$ and $H_r$ components in the near-zone, (4) and (5), and in the far-zone (10) and (11).

Figures 17 and 18 show the experimental data of $H_\phi$ and $H_r$ as functions of $\rho$ compared to the theoretical expressions for the static-zone, near-zone, and far-zone. As in Figure 16, there is no overlap of the theories for the static-zone and the near-zone. The deviation of the experimental curve from the theoretical curves is caused by two effects: (1) the receiving antenna transmission line distorted the field measured by the receiving antenna, and (2) the receiving antenna, when detecting the field in the static-zone and the near-zone does not "see" the transmitting antenna as a point source. However, these two disturbances were not severe enough to seriously alter the experimental data in this case.

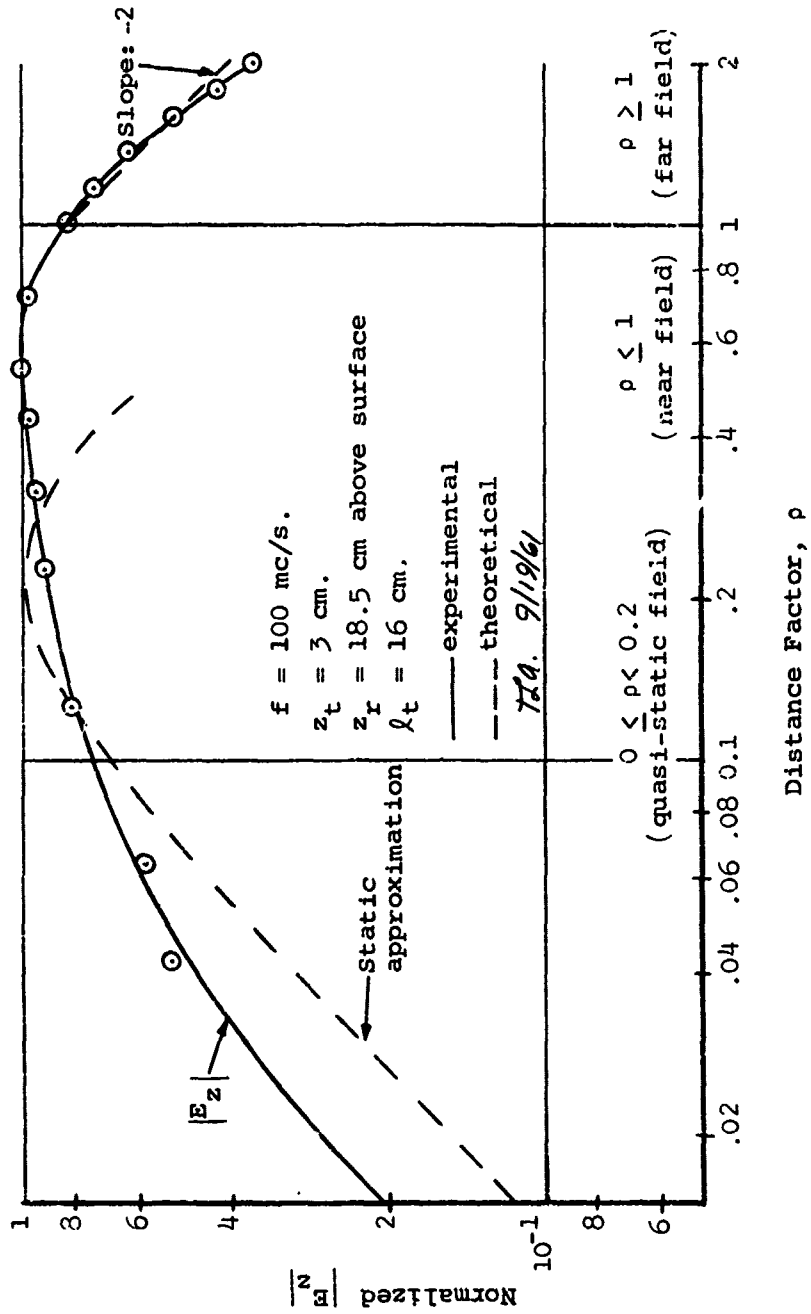


Figure 16--Variation of the maximum magnitude of the electric field component, $E_z$, in air with radial distance in units of free-space-wavelength/$2\pi$

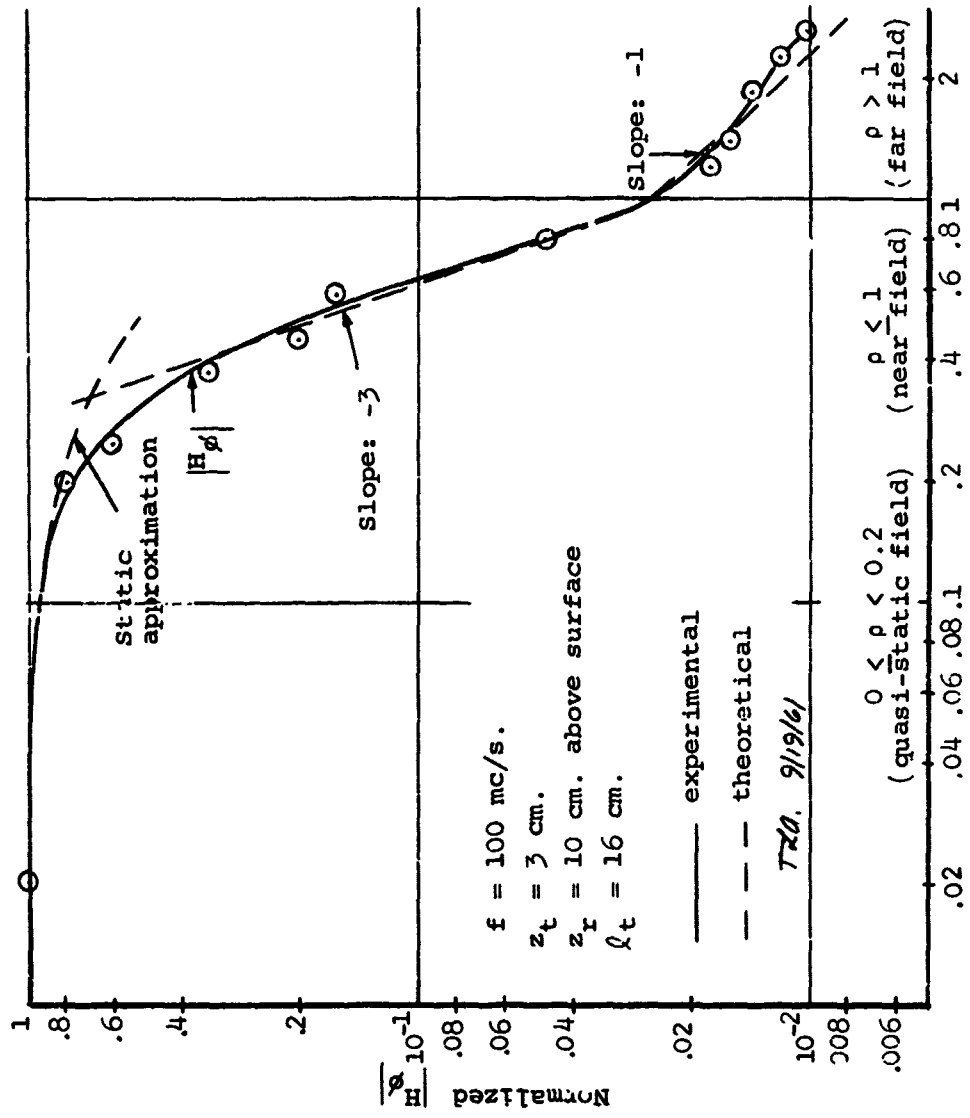


Figure 17--Variation of the maximum magnitude of the magnetic field component, Hø, in air with radial distance in units of free-space-wavelength/$2\pi$

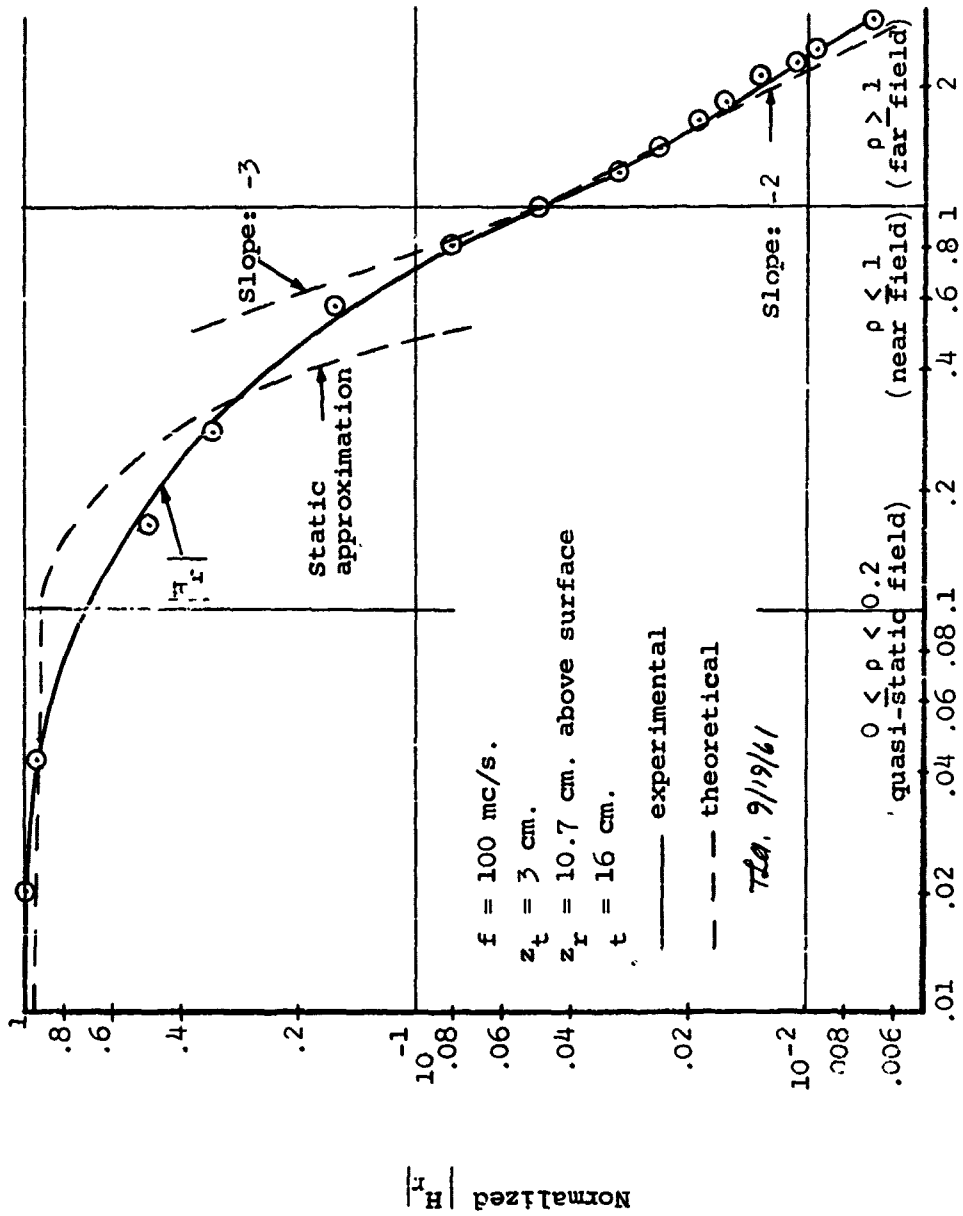


Figure 18--Variation of the maximum magnitude of the magnetic field component, $H_r$, in air with radial distance in units of free space-wavelength/$2\pi$.

## 5.0 Conclusions

The three results of the experimental work are the following:

(1) A laboratory-size model system and a technique were developed for measuring scaled variations of the electric and magnetic field components with frequency, properties of the conducting medium, relative position and orientation between transmitting and receiving antennas, and various model antenna shapes and designs.

This model requires that the antenna be scaled satisfactorily in size and frequency such that the theory of operation of the antenna under actual conditions can be used to describe its operation under scaled conditions. If the theory is valid and the antenna can be physically scaled, then the model system can be used for frequency scaling ($f \leq 400$ mc/s).

(2) To determine the capabilities and limitations of this modeling system, variations of the $E_r$ and $E_\phi$ electric field components, for both near-zone and far-zone fields in the sea, were determined with respect to the following variables:

(i) separation between transmitting and receiving antennas, $\rho$;

(ii) depth of transmitting and/or receiving antennas, $z$;

(iii) angular orientation of transmitting and/or receiving antennas, $\phi$;

(iv) length of transmitting antenna, $\ell$;

(v) dipole current, I;

(vi) conductivity of salt water, $\sigma$;

(vii) frequency (for five selected frequencies, giving $S_1$, scaling factors, from $2.5 \times 10^{-4}$ to $2.5 \times 10^{-5}$).

The results have been graphed and can be summarized as follows:

(i) $E_r$ varies as $\rho^{-3}$ in near-zone
$\rho^{-1}$ in far-zone
$E_\phi$ varies as $\rho^{-3}$ in near-zone
$\rho^{-2}$ in far-zone

(ii) $E_r$, $E_\phi$, and all other field components vary as $\exp(-z/\delta)$ with $\delta$ being skin depth.

(iii) $E_r$ varies as cos $\phi$, and $E_\phi$ varies as sin $\phi$.

(iv) $E_r$, $E_\phi$, and all other field components vary linearly with I and $\ell$.

(v) The field components vary in a complicated manner with f and $\sigma$. These two parameters were not checked independently, but were indirectly checked during the other tests. Most of the tests, however, we conducted with f = 100 mc/s and $\sigma \approx 4$ mhos/m. The $E_z$ and $H_z$ field components in the sea are negligible compared to the transverse electric and magnetic field components.

This set of tests was used because the theoretical results, used as a comparison for the experimental results presented here, have been predicted by Norgorden, Moore, Baños and Wait, and are accepted by investigators in VLF research. The fact that the theoretical and experimental results agree as well as they do is strong indication that both are quite accurate, because the chance that both results can be in such agreement, and be incorrect, is certainly negligible. There was no serious deviation of the experimental data from the theory over

the valid range of variations of the parameters. In fact, the experimental data agreed with the theory often beyond the valid range of variations, implying that some of the theoretical restrictions are more conservative than necessary.

(3) In addition to the $E_r$ and $E_\phi$ components in the sea, the $H_\phi$, $H_r$, and $E_z$ components for the static-zone, near-zone, and far-zone fields in the air were measured as a function of $\rho$, all other parameters being held constant. The results have been graphed and are summarized as follows:

$E_z$ varies as: $\rho$ in static-zone, independent of frequency; and reaches a maximum at $r = z'/2$.
$\rho^{-2}$ in near-zone.
$\rho^{-1}$ in far-zone.

$H_\phi$ varies as: constant in static-zone, independent of frequency; and reaches a maximum at $r = 0$.
$\rho^{-3}$ in near-zone.
$\rho^{-1}$ in far-zone.

$H_r$ varies as: constant in static-zone, independent of frequency; and reaches a maximum at $r = 0$.
$\rho^{-3}$ in near-zone.
$\rho^{-2}$ in far-zone.

The experimental data agreed reasonably well with the theoretical data over the ranges of validity. Some field distortion was caused by (1) the receiving antenna transmission line coupling the antenna to the receiver, and (2) in the

static-zone the antennas were too close together for the transmitting antenna to appear as a point source.

This model, while not at all new in concept, may be used effectively to measure scaled propagation patterns and impedances of various submerged transmitting antennas. The principal advantage of this model system is its small (laboratory) size, hence: one can expect relatively easily controlled experimental variables, smaller antennas, lower power requirements, and probably less expense than in the case of a larger model or full scale experiment. The principal disadvantage is the high frequency (small scaling factor), hence: some antennas cannot be modeled at such a high (VHF) frequency and the theory describing the VLF radiation from the antennas may not be valid at VHF.

## APPENDIX

### Details and Specifications of Model

**Tank:** 11.5' diameter x 2' deep.

- **tank wall:** Five weatherized masonite panels, 1/4" x 2' x 8', bolted together.
- **tank liner:** Polyethelene liner, 0.08" thick, fabricated for a cylindrical tank 12' diameter x 2.5' deep.
- **capacity:** 208 cu. ft., 1550 gallons; 7-1/2 tons of salt water.
- **solution:** Variation of conductivity from 3 mhos/m to 5 mhos/m; i. e., from 400 to 500 lbs of granulated 99.9% NaCl dissolved in water.

**Crossbeam:** Choice redwood beam, 2" x 4" x 16', supported by two end frames constructed from 2" by 4" pine.

**Slide blocks:** Constructed from nylon and phenolic plastic stock.

**Pulley System for positioning slide blocks:** Constructed using nylon pulleys and 1/8" nylon cord.

**Coaxial antenna:** Constructed from RG 142/U coaxial cable.

- **inner conductor:** Silvered copperweld; diameter, a = 0.912 mm.
- **dielectric:** Teflon ($\epsilon_r = 2.06$); diameter, b = 2.94 mm.
- **outer conductor:** Silvered copper braid.

b/a = 3.24

insulation: Tape moisture seal, single fiber glass.

braid: Silicone-varnish impregnated.

characteristic impedance of cable: $Z_o$ = 50 ohms.

overall diameter: 5.23 mm. (nominal).

Transmitting equipment: (1) Hewlett-Packard VHF signal generator model 608c (freq. range 10-480 mc/s; maximum power out, 20 mw = 1 volt across 50 ohms); (2) General Radio VHF signal generator model 1021 (freq. range 40-250 mc/s; maximum power out, 80 mw = 2 volts across 50 ohms.)

Receiving equipment: Stoddard Aircraft VHF radio interference field intensity meter model NM-30A (freq. range 20-400 mc/s; maximum sensitivity one microvolt across 50 ohms). Remote meter was used with 20' connecting cable.

## REFERENCES


Appleman, C. B., Naval Research Laboratory, Report No. 3889, SECRET (1951).

Baños, A., Jr., and J. P. Wesley, The horizontal dipole in a conducting half-space, Univ. of Calif. Marine Physical Laboratory, Reports No. 53-33 (1953) and No. 54-33(1954).

Flath, E. H., Jr., and O. Norgorden, Expressions for input impedance and power dissipation in lossy concentric lines, Naval Research Laboratory Report No. R3436 (1949).

Fratianni, S. V., Submerged VLF reception: a study of various loop coupling methods, Naval Research Laboratory Report No. 2872 (1946).

Fratianni, S. V., Theory and design of resonant transformer-coupled loop-antenna input systems for VLF reception, Naval Research Laboratory Report No. R-3281 (1948).

Isel, F. C., Test of underwater reception of low frequency radio signals, Naval Research Laboratory Report No. R-1717 (1941).

Kraichman, M. B., Basic experimental studies of the magnetic field from electromagnetic sources immersed in a semi-infinite conducting medium, J. Research NBS 64D (Radio Prop.), No. 1, 21-25 (Jan. 1960).

Moore, R. K., The theory of radio communication between submerged submarines, Ph. D. Thesis, Cornell Univ. (1951).

Moore, R. K., and W. E. Blair, Dipole radiation in a conducting half space, J. Research NBS 65D, No. 6. 547-63 (1961).

Musselman, M. L., Naval Research Laboratory Report No. 4180 CONFIDENTIAL (1953).

Musselman, M. L., and G. W. Roos, Naval Research Laboratory Report No. 4537 CONFIDENTIAL (1955).

Norgorden, O., The submerged reception of radio frequency signals, Naval Research Laboratory Report No. R-1669 (1940).

Quinn, R. B., and O. Norgorden, Naval Research Laboratory Report No. R-3006 CONFIDENTIAL (1946).

Rauen, T. J., Naval Research Laboratory Report No. 4250 Confidential (1953).

Saran, G. S., and G. Held, Field strength measurements in fresh water, J. Research NBS 64D, (Radio Prop.), No. 5, 425-7, (1960).

Snodgrass, J. M., and P. Rudnick, Univ. of California, Scripps Institute of Oceanography Report S1054-30 CONFIDENTIAL (1954).

Sommerfeld, A., Über die Ausbreitung Elektromagnetischer Wellen über ein eben Erde, Ann. der Phys. Ser. 4, 28, 665-736, (1909).

Sommerfeld, A., Über die Ausbreitung der Wellen in der drahtlosen Telegraphie, Ann. der Phys. Ser. 4. 81, 1135-53 (1926).

Wait, J. R., The electromagnetic fields of a horizontal dipole in the presence of a conducting half-space, Canadian J. Physics 39, 1017-28 (1961).

Weyl, H., Ausbreitung elektromagnetischer Wellen über einem ebener Leiter, Ann. der Phys. Ser. 4, 60, 481-500 (1919).

Distribution List for Unclassified Section
of Progress Report
Contract Nonr 2798(01)

| Addressee | No. of Copies |
|---|---|
| Director, Armed Services Technical Information Agency<br>Arlington Hall Station<br>Arlington, Virginia | 10 |
| Director<br>Naval Research Laboratory<br>Code 5360 - Code 5420 - Code 2027<br>Washington 25, D. C. | 5 |
| Commanding Officer and Director<br>Naval Electronics Laboratory<br>San Diego 52, California | |
| Director Special Projects (SP204)<br>Bureau of Naval Weapons<br>Washington 25, D. C. | |
| Commander<br>US Naval Ordnance Test Station<br>3202 East Foothill Blvd.<br>Pasadena 8, California | |
| Commanding Officer and Director<br>US Navy Underwater Sound Laboratory<br>New London, Conn.<br>ATTN: Mr. C. B. Dunn | 2 |
| Chief of Bureau of Ships<br>Navy Department<br>Code 671C<br>Code 679<br>Code 686<br>Code 687A<br>Code 687H<br>Washington 25, D.C. | 5 |
| Chief of Naval Operations<br>Op 08 — 1<br>Op 94T — 2<br>Navy Department<br>Washington 25, D. C. | 3 |
| Chief of Naval Research<br>Code 466 — 3<br>Code 427 — 1<br>Navy Department<br>Washington 25, D. C. | 4 |

Electrical Engineering Research
Document File
School of Electrical Engineering
Ithaca, New York 1

Mr. Albert R. Giddis
Project Engineer
Advance Programs Section
Philco Corporation
Western Development Labs.
3875 Fabian Way
Palo Alto, California 1

Mr. Richard C. Becker
Senior Staff Engineer
Amphenol-Borg Electric Corporation
25th Avenue at Cermak
Broadview, Illinois 1

Mr. Harold A. Wheeler
Wheeler Laboratories, Inc.
122 Cutter Miller Road
Great Neck, New York 1

Mr. J. Y. Wong
Antenna Group (Microwave Section)
National Research Council of Canada
Ottawa 2, Ontarie, Canada 1

Stanford Electrical Laboratories
Stanford University
Stanford, California 1

Development Engineering Co.
ATTN: Mr. Don Watt
Boulder, Colorado 1

Development Engineering Company
ATTN; Mr. Lucien Rawls
Leesburg, Virginia 1

Space Electronics Corporation
1200 AirWay
Glendale 1, California
ATTN; Mr. Frank W. Lehan 1

Stromberg-Carlson
Div. of General Dynamics
Rochester, New York
ATTN; Victor Savchuk 1

Com. Officer and Director
US Navy Underwater Sound Lab.
Fort Trumbull
New London, Connecticut
ATTN: Mr. G. M. Milligan — 1

Com. Officer and Director
US Naval Ordnance Lab.
Corona, California
ATTN: Mr. A. W. Walters
Code 45 — 1

Technical Director
US Naval Ordnance Test Station
China Lake, California — 1

Com. Officer and Director
US Naval Ordnance & Lab.
White Oak, Maryland
ATTN: Mr. Robert Miller
Code 042 — 1

Applied Physics Laboratory
Johns Hopkins University
ATTN: Cdr. Pollow
8621 Georgia Avenue
Silver Springs, Md. — 1

Director
Woods Hole Oceanographic Institution
Woods Hole, Mass.
ATTN: Dr. Hersey — 1

Dr. Kenneth A. Norton, Chief
Radio Propagation Engr. Division
Central Radio Prop. Lab.
National Bureau of Standards
Boulder, Colorado — 1

National Research Council
Com. on Undersea Warfare
2101 Constitution Ave., N. W.
Washington 25, D. C. — 1

Dr. J. R. Wait, Consultant
Central Radio Prop. Lab.
National Bureau of Standards
Boulder, Colorado — 2

Hoffman Radio
F. A. Schor, Unit Supervisor
Communication Section
P. O. Box 2471
Los Angeles 54, California — 1

P. S. Carter
Radio Corporation of America
Rocky Point, L. I., New York 1

Dr. J. H. Mulligan, Jr.
Chairman, Electrical Engr. Department
New York University
New York 53, New York 1

Mr. Loren S. Bearce
Code 5423
Naval Research Laboratory
Washington 25, D. C. 1

The Mitre Corporation
Middlesex Turnpike
Bedford, Massachusetts
ATTN: Mr. Karl Swartzel 1

Dr. Ronald V. Row
Sylvania Elec. Systems
Division of Sylvania Elec. Products, Inc.
100 First Avenue
Waltham 54, Massachusetts 1

Mr. E. L. Sanderson
US Naval Mine Detection Laboratory
Panama City, Florida 1

Dr. L. Katz
Applied Physics Laboratory
Johns Hopkins University
Silver Springs, Maryland 1

Program Director
Advance Science Programs
National Science Foundation
1951 Constitution Avenue
Washington 25, D. C. 1

Mr. Walter N. Phillips
Research Division Electronic Communications Inc.
1830 York Road
Timonium, Maryland

Mr. L. H. Rorden
Stanford Research Institute
Menlo Park, California 1

Mr. Martin Katzin
Electromagnetic Research Corporation
5001 College Avenue
College Park, Maryland 1

Mr. Martin B. Kraichman
Naval Ordnance Lab.
White Oaks, Maryland 1

Ordnance Research Laboratory
Pennsylvania State College
P. O. Box 30
State College, Pa. 1

Director
Scripps Institution of Oceanography
La Jolla, California 1

Director, Hudson Laboratories
Columbia University
P. O. Box 329
Dobbs Ferry, New York 1

Dr. Cullen Crain
Rand Corporation
Santa Monica, California 1

University of Chicago
Laboratories for Applied Science
Museum of Science
Chicago 37, Ill.
ATTN: Mr. Van Zeelind 1

Commanding Officer
Office of Naval Research
Branch Office
1030 East Green Street
Pasadena 1, California 3

National Science Foundation
Engineering Program
Washington 25, D. C. 1

Director
Research Lab. of Elec.
Massachusetts Institute of Technology
Cambridge 39, Mass. 1

Dr. R. W. P. King
Cruft Laboratory
Harvard University
Cambridge 38, Mass. 1

Dr. R. H. Duncan
Physical Science Laboratory
New Mexico State University
University Park
Las Cruces, New Mexico 1

Dr. B. M. Fannin
Electrical Engineering Research Laboratory
University of Texas
Austin 3, Texas 1